(4)

TECHNICAL REPORT BRL-TR-3083

BRL

ANALYSIS OF THE FLIGHT PERFORMANCE OF THE 155 MM M864 BASE BURN PROJECTILE

JAMES E. DANBERG

APRIL 1990

U.S. ARMY LABORATORY COMMAND

BALLISTIC RESEARCH LABORATORY
ABERDEEN PROVING GROUND, MARYLAND

NOTICES

Destroy this report when it is no longer needed. DO NOT return it to the originator.

Additional copies of this report may be obtained from the National Technical Information Service, U.S. Department of Commerce, 5285 Port Royal Road, Springfield, VA 22161.

The findings of this report are not to be construed as an official Department of the Army position, unless so designated by other authorized documents.

The use of trade names or manufacturers' names in this report does not constitute indorsement of any commercial product.

REPORT DOCUMENTATION PAGE

Form Approved
OMB No. 0704-0188

1. AGENCY USE ONLY (Leave blank)	2. REPORT DATE	3. REPORT TYPE AND DATES COVERED
	April 1990	Technical

4. TITLE AND SUBTITLE

ANALYSIS OF THE FLIGHT PERFORMANCE OF THE 155 MM M864 BASE BURN PROJECTILE

5. FUNDING NUMBERS

1L162618AH80
62618A 00 001 AJ

6. AUTHOR(S)

JAMES E. DANBERG

7. PERFORMING ORGANIZATION NAME(S) AND ADDRESS(ES)

8. PERFORMING ORGANIZATION REPORT NUMBER

9. SPONSORING / MONITORING AGENCY NAME(S) AND ADDRESS(ES)

Ballistic Research Laboratory
ATTN: SLCBR-DD-T
Aberdeen Proving Ground, MD 21005-5066

10. SPONSORING / MONITORING AGENCY REPORT NUMBER

BRL-TR-3083

11. SUPPLEMENTARY NOTES

12a. DISTRIBUTION / AVAILABILITY STATEMENT

Approved for public release; distribution is unlimited.

12b. DISTRIBUTION CODE

13. ABSTRACT *(Maximum 200 words)*

An engineering model has been developed to compute the flight performance of the M864 base burn projectile. This model includes the coupled performance of the gas generator, effects of injected mass flow on the aerodynamics, and a modified point mass trajectory simulation. The gas generator model is based on measured burn rates and basic fluid dynamics. The discharge rate of the generator is calibrated against laboratory experiments. Effects of spin on burn rate are deduced from comparison of analysis with spin fixture tests. Linear and first order non-linear effects of mass injection on base pressure are the basis for evaluation of base drag. Navier-Stokes solutions near the base with air injection provides essential data. Correlation equations predict base pressure as a function of Mach number, injection rate, and propellant gas temperature. Temperature effects on base pressure are a unique feature of the analysis.

The base bleed model has been applied to an instrumented flight test case with good qualitative agreement. There is disagreement with burnout measurements of four percent at low altitudes and a much stronger dependence on elevation than observed in flight. The technique predicted range within four percent.

14. SUBJECT TERMS

Injection of Combustion Products, Base Burn, Base Bleed, Spin, Trajectory, Navier-Stokes Computations, and Solid Propellant

15. NUMBER OF PAGES

56

16. PRICE CODE

17. SECURITY CLASSIFICATION OF REPORT	18. SECURITY CLASSIFICATION OF THIS PAGE	19. SECURITY CLASSIFICATION OF ABSTRACT	20. LIMITATION OF ABSTRACT
UNCLASSIFIED	UNCLASSIFIED	UNCLASSIFIED	UL

NSN 7540-01-280-5500

Standard Form 298 (Rev 2-89)
Prescribed by ANSI Std Z39-18
298-102

GENERAL INSTRUCTIONS FOR COMPLETING SF 298

The Report Documentation Page (RDP) is used in announcing and cataloging reports. It is important that this information be consistent with the rest of the report, particularly the cover and title page. Instructions for filling in each block of the form follow. It is important to *stay within the lines* to meet *optical scanning requirements*.

Block 1. Agency Use Only *(Leave blank)*.

Block 2. Report Date. Full publication date including day, month, and year, if available (e.g. 1 Jan 88). Must cite at least the year.

Block 3. Type of Report and Dates Covered. State whether report is interim, final, etc. If applicable, enter inclusive report dates (e.g. 10 Jun 87 - 30 Jun 88).

Block 4. Title and Subtitle. A title is taken from the part of the report that provides the most meaningful and complete information. When a report is prepared in more than one volume, repeat the primary title, add volume number, and include subtitle for the specific volume. On classified documents enter the title classification in parentheses.

Block 5. Funding Numbers. To include contract and grant numbers; may include program element number(s), project number(s), task number(s), and work unit number(s). Use the following labels:

C	- Contract	PR	- Project
G	- Grant	TA	- Task
PE	- Program Element	WU	- Work Unit Accession No.

Block 6. Author(s). Name(s) of person(s) responsible for writing the report, performing the research, or credited with the content of the report. If editor or compiler, this should follow the name(s).

Block 7. Performing Organization Name(s) and Address(es). Self-explanatory.

Block 8. Performing Organization Report Number. Enter the unique alphanumeric report number(s) assigned by the organization performing the report.

Block 9. Sponsoring/Monitoring Agency Name(s) and Address(es). Self-explanatory.

Block 10. Sponsoring/Monitoring Agency Report Number. *(If known)*

Block 11. Supplementary Notes. Enter information not included elsewhere such as: Prepared in cooperation with...; Trans. of...; To be published in.... When a report is revised, include a statement whether the new report supersedes or supplements the older report.

Block 12a. Distribution/Availability Statement. Denotes public availability or limitations. Cite any availability to the public. Enter additional limitations or special markings in all capitals (e.g. NOFORN, REL, ITAR).

- DOD - See DoDD 5230.24, "Distribution Statements on Technical Documents."
- DOE - See authorities.
- NASA - See Handbook NHB 2200.2.
- NTIS - Leave blank.

Block 12b. Distribution Code.

- DOD - Leave blank.
- DOE - Enter DOE distribution categories from the Standard Distribution for Unclassified Scientific and Technical Reports.
- NASA - Leave blank.
- NTIS - Leave blank.

Block 13. Abstract. Include a brief *(Maximum 200 words)* factual summary of the most significant information contained in the report.

Block 14. Subject Terms. Keywords or phrases identifying major subjects in the report.

Block 15. Number of Pages. Enter the total number of pages.

Block 16. Price Code. Enter appropriate price code *(NTIS only)*.

Blocks 17 - 19. Security Classifications. Self-explanatory. Enter U.S. Security Classification in accordance with U.S. Security Regulations (i.e., UNCLASSIFIED). If form contains classified information, stamp classification on the top and bottom of the page.

Block 20. Limitation of Abstract. This block must be completed to assign a limitation to the abstract. Enter either UL (unlimited) or SAR (same as report). An entry in this block is necessary if the abstract is to be limited. If blank, the abstract is assumed to be unlimited.

TABLE OF CONTENTS

INTENTIONALLY LEFT BLANK.

LIST OF FIGURES

LIST OF TABLES

INTENTIONALLY LEFT BLANK.

ACKNOWLEDGMENT

The author wishes to express his appreciation to a number of people who have provided data and critical reviews and helpful discussions as this work progressed.

Mr. Charles Nietubicz and Dr. J. Sahu provided the essential data from their Navier-Stokes computations of the M864. Ms. R. Larkin ran many additional special cases.

Dr. A. Kotlar gave very valuable suggestions and critical comments on the geometry of the propellant grain calculation and Dr. J. Kuzan was responsible for some of the initial work on this topic.

Mr. L. Kayser's experiments on the various aspect of the M864 were essential in formulating and quantifying the present model. His wind tunnel measurements on the base bleed effect on base pressure were most valuable in recognizing the nearly linear relationship between mass flow and pressure. The attempt to interpret his more recent ground based spin fixture tests formed the start point for the formulation of the model. Finally, his most recent flight test provided the data for evaluation of the model.

The modified point mass trajectory simulation model is based on the work of Mr. R. Lieske. He critically reviewed the report and furnished the results of his flight tests. His many discussions on the M864 were very important and helpful.

INTENTIONALLY LEFT BLANK.

I. INTRODUCTION

The primary objective in this work is to develop an engineering analysis model for the M864 base bleed/burn projectile flight performance. This model includes analyses of all three elements of the problem; namely: gas generation, effect of bleed on aerodynamic drag, and a trajectory model. Because each of the above elements is time dependent, all three elements must be solved simultaneously. This is in contrast with the conventional projectile where the aerodynamic coefficients can be determined independent of any specific trajectory. The analysis will be based on much of the existing experimental and numerical data obtained as part of the M864 program. However, the techniques developed are easily adapted to other designs.

A secondary objective is to determine how the numerical solutions to the Navier-Stokes equation can be applied to the problem. At present these computations do not account for the time dependent nature of the gas generator and changing free-stream conditions along the trajectory. Furthermore, the codes used in these studies do not provide for gas properties different from air which is treated as a perfect gas. Thus, steady state solutions are obtained for specific free-stream conditions with equivalent air mass flow and temperature imposed as boundary conditions at the exit of the gas generator. The results of these computations are correlations of base pressure as a function of injected mass flow and temperature.

II. BACKGROUND LITERATURE

A broad survey of the aerodynamics of base bleed/burn was performed for a meeting in 1974.[1] The Proceedings of that meeting contained an extensive bibliography of work reported to that time. Since 1974, much new work has been carried out, particularly in developing and testing practical projectile designs using base burn, such as the U.S. Army's M864.[2,3,4,5,6,7,8,9] Figure 1 shows the configuration of the M864 and describes its physical properties. The National Defense Research Institute (FOA) of Sweden also has developed a family of projectiles[10,11,12,13,14] similar to the M864. They have published a number of reports describing their analytical techniques used in the projectile design. The work of Gunners, Andersson, and Hellgren[14] provides the most comprehensive discussions of their results. The analysis developed at BRL is quite similar to the Swedish work and to that of Hudgins[15] except for the use of Navier-Stokes computations to evaluate the effects of bleed on the base pressure and drag. The results of the laboratory spin fixture tests also permit a more detailed analysis of the gas generator performance than has been possible previously. Additional references to the current international base bleed/burn projectile literature are contained in the Proceedings of the First International Symposium on Base Bleed[16] and in other journal reports. [17,18,19,20,21,22] Additional recent studies specifically directed at combustion in the wake are contained in the work of Schetz, et al,[23,24,25] Hubbartt, Strahle, Neale and their co-workers,[26,27,28,29] and Schadow and Chieze.[30,31]

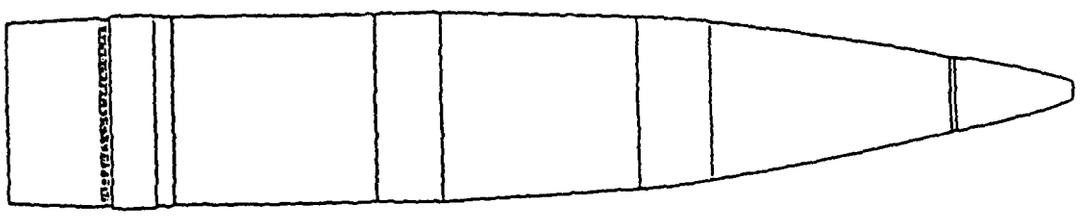

Dimensions

Length of Projectile	calibers	5.79
Nose Length	calibers	3.42
Cylinder Length	calibers	1.86
Boattail Length	calibers	.50
Boattail Angle	degrees	3.00

Mass Properties

Mass	kgs	46.95
	(lbs)	103.5
Mass of Fuel	kgs	1.21
	(lbs)	2.67
Center of Gravity	cm from nose	58.8
	(in from nose)	23.16
Moments of Inertia		
Axial	$kg\text{-}m^2$	.158
	$(lb\text{-}ft^2)$	3.75
Transverse	$kg\text{-}m^2$	1.657
	$(lb\text{-}ft^2)$	39.32

Figure 1: Physical Characteristics of the 155mm, DPICM, M864 Projectile

III. GAS GENERATOR

The gas generator for the M864 base bleed projectile is housed in the afterbody which is shown in cross section in Figure 2. The gas generator consists of two identical solid propellant grains as shown in Figure 3. These two elements provide an inner cylindrical burning surface and four planer surfaces separated by a 3 mm slot. The slot is held open during launch by four spacers. In these calculations the regression rates on the cylindrical surface and on the slot surfaces are assumed uniform over the surfaces but not necessarily equal.

The geometry of the grain shown in Figure 3 can be described in terms of five dimensions (initial dimensions are designated with subscript i):

l_i=the maximum length of the grain

r_i=the inner radius of the cylindrical center hole

r_{mx}=the maximum radius of the grain

r_s=the radius of the curved ends of the cylinder

w_i=the half thickness of the slot

Measurements of the propellant (designated AP-2) burning rate have been obtained by Miller and Holmes[32] using a strand burning technique. Tests were performed over a range of chamber pressures and the results are shown in Figure 4. The strand burning rate, $\dot{r}_o$, can be written as:

$$\dot{r}_o = kP_c^n \tag{1}$$

where P_c is in bars. The values found by Miller for the AP-2 propellant are: k=0.0009132 m/s and n=0.6655.

Let the burning rate on the cylindrical surface be $\dot{r}_c$ and on the slot surface be $\dot{r}_s$. The radius change of the cylinder at any instant is:

$$dr = \dot{r}_c dt,$$

and the regression of the slot is:

$$dw = \dot{r}_s dt = \frac{\dot{r}_s}{\dot{r}_c} dr.$$

If the ratio $\frac{\dot{r}_s}{\dot{r}_c}$ is a constant throughout the burn, then the burning surface areas, a_c and a_s, can be defined in terms of r, the cylinder radius. The formulas which are used to compute the surfaces at any instant, where the cylindrical surface radius is r, are:

$$a_c = [2\pi - 4\sin^{-1}(\frac{w}{r})]rl, \tag{2}$$

where:

$$l = l_i - 2\left[r_s - \sqrt{r_s^2 - (r_s - r_{mx} + r)^2}\right](1 - j),$$

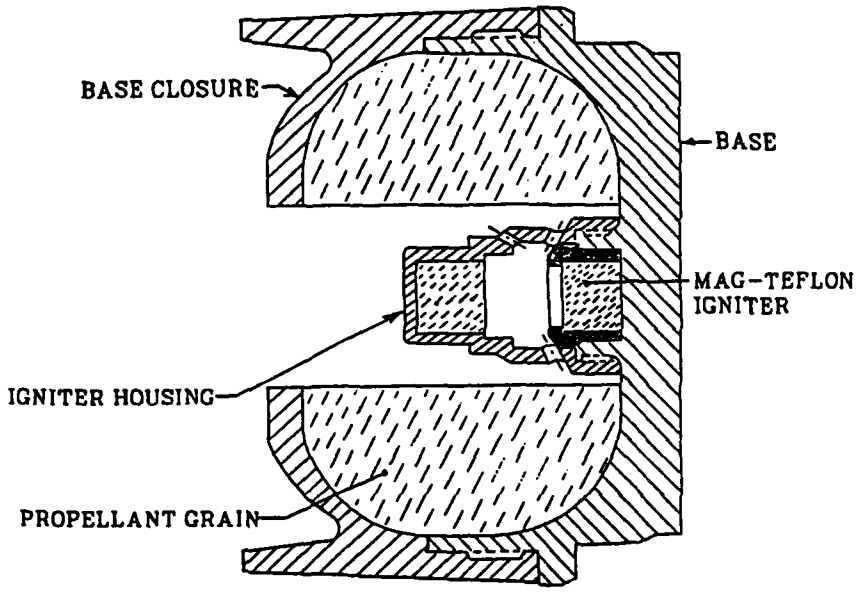

Figure 2: Base, Propellant, Igniter for M864

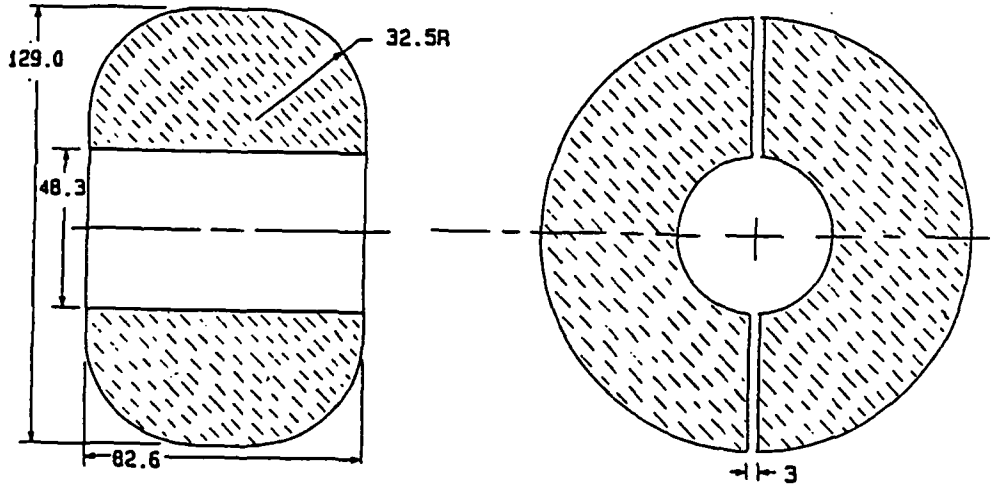

Figure 3: Propellant Grain Geometry

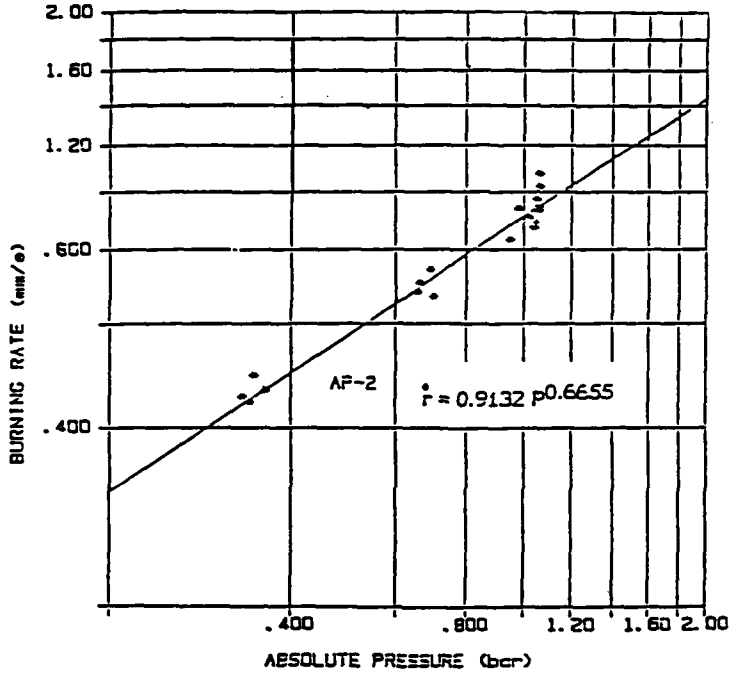

Figure 4: Experimental Strand Burning Rate, (Ref. 32)

$$w = w_i + \frac{\dot{r}_s}{\dot{r}_c}(r - r_i),$$

and,

$$r \leq (r_{mx} - r_s) \ \ then \ \ j = 1,$$
$$r > (r_{mx} - r_s) \ \ then \ \ j = 0.$$

The slot area can be computed from:

$$a_s = 4a_{s1} + 8a_{s2} + 8a_{s3}, \tag{3}$$

where,

$$a_{s1} = (l_i - 2r_s)(\sqrt{r_{mx}^2 - w^2} - \sqrt{r^2 - w^2}), \tag{4}$$

$$a_{s2} = r_s(\sqrt{(r_{mx} - r_s)^2 - w^2} - \sqrt{r^2 - w^2})j, \tag{5}$$

$$a_{s3} = \int_{\sqrt{\bar{r}^2 - w^2}}^{\sqrt{r_{mx}^2 - w^2}} \left[r_s^2 - \left(\sqrt{z^2 + w^2} - r_{mx} + r_s\right)^2\right]^{\frac{1}{2}} dz, \tag{6}$$

and where $\bar{r} = r$ unless

$$r < (r_{mx} - r_s) \ \ then \ \ \bar{r} = (r_{mx} - r_s).$$

Note that in equation 6, the integral can not be written in closed form and thus it has been evaluated numerically using the trapezoidal rule. This area is the contribution from the curved end corners of the grain.

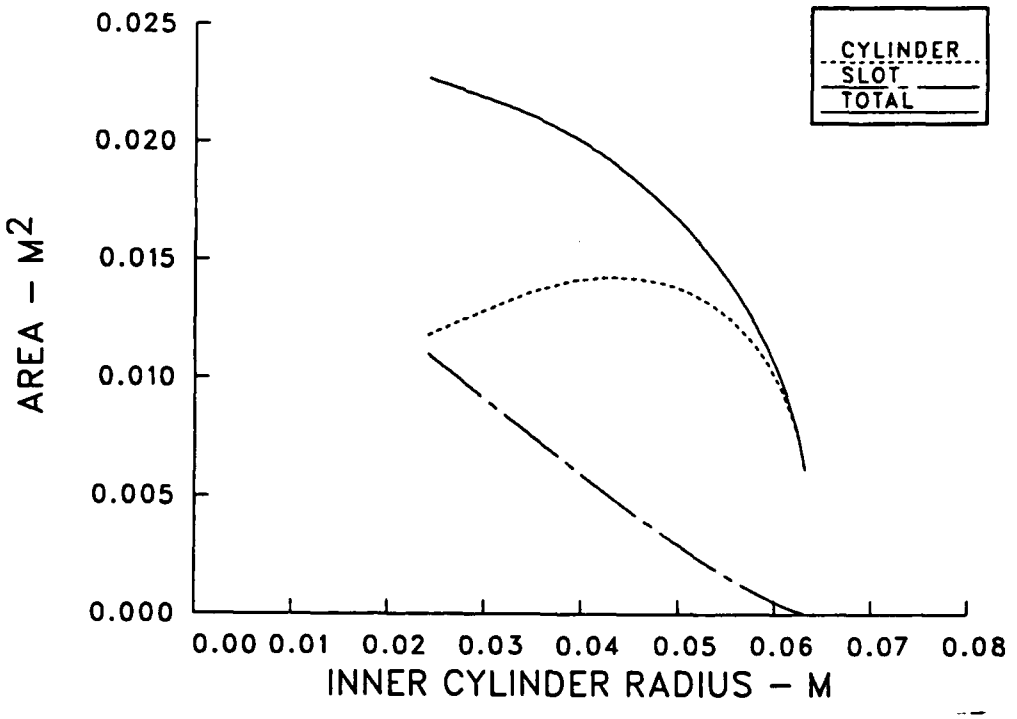

Figure 5: Grain Burning Surface Areas As A Function of Cylindrical Radius

Figure 5 shows the two surfaces a_c and a_s and their sum for the M864 grain assuming the special case of $\dot{r}_c = \dot{r}_s$. Note that the mass flow generated by the burning propellant is:

$$\dot{m} = \rho_s[a_c\dot{r}_c + a_s\dot{r}_s] \tag{7}$$

where ρ_s is the solid propellant density (AP-2 propellant ρ_s=1532.0 kg/m^3).

1. TESTS IN A GROUND BASED SPIN FIXTURE

Tests of the gas generator have been performed in ground facilities where an actual motor was mounted on a spin fixture.[5] These tests measured the chamber temperature, chamber pressure and burn time for various rates of spin as shown in Figures 6 and 7 and Table 1, respectively.

The following section analyzes these tests in an attempt to show that simple analytical relationships describe the performance of the gas generator. The gas generator output mass flow depends on the chamber pressure, the pressure into which it exhausts, time and spin rate. The measured chamber pressure-time histories, indicate to this author, that there is a difference between the burning rate on the cylindrical surface and on the surface of the slot. The chamber pressure is directly an indication of the exit mass flow. If the burning rates are equal on the two surfaces then the chamber pressure should decrease monotonically with time, after an initial transient. This is indicated in Figure 5 and for the zero spin case in Figure 7. As shown in Figure 7, at high spin rates the pressure initially increases and

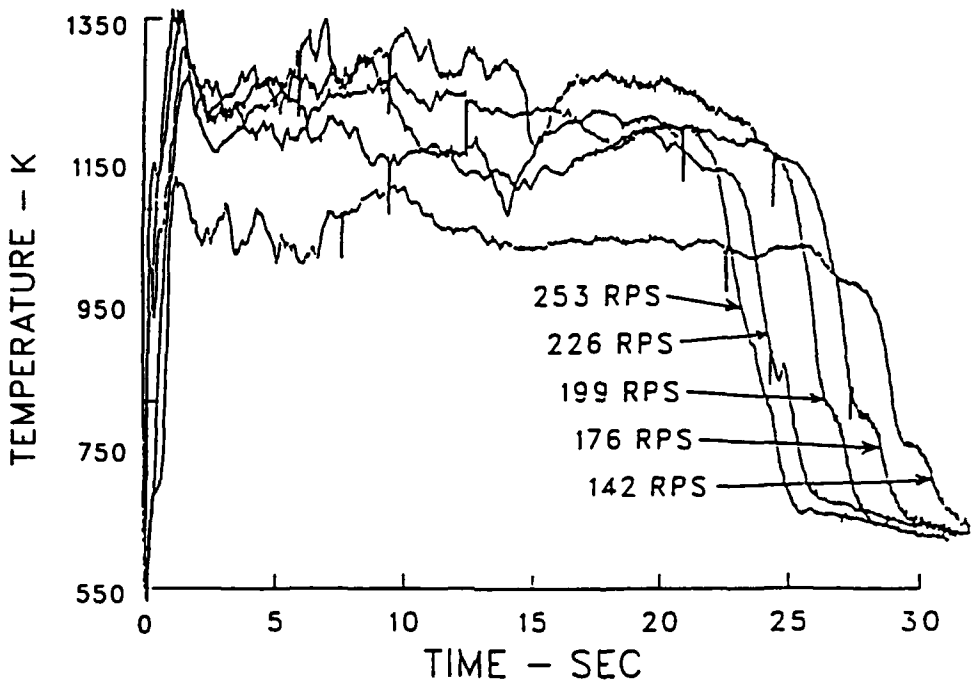

Figure 6: Chamber Temperature Measurements, AP-2 Propellant, (Ref. 5)

then falls off, indicating that the cylindrical surface is more important in determining the mass flow, and thus chamber pressure than the monotonically varying slot contribution. To show this more explicitly consider the following analysis.

The mass flow is assumed subsonic and a modified form of the incompressible Bernoulli equation is applied:

$$P_c - P_e = \frac{1}{C_v^2} \frac{\rho_e^2 u_e^2}{2\rho_e}$$

TABLE 1: SPIN FIXTURE BURN TIME DATA - AP-2 PROPELLANT

RUN	SPIN RPS	BURN TIME SEC.
2	0	40.0
3	99	31.9
4	142	29.0
5	176	27.4
6	199	26.0
7	226	23.9
8	253	22.8

(where C_v is a discharge coefficient) along with the continuity equation:

$$\dot{m} = \rho_e u_e A_e$$

which can be combined to give:

$$\dot{m} = \left\{ C_v A_e \sqrt{2\rho_e P_e} \right\} \sqrt{\frac{P_c}{P_e} - 1}. \tag{8}$$

The discharge coefficient is assumed to be constant in this case. Initially when the radius of the grain equals the orifice radius, there are negligible orifice losses and C_v is infinite. This corresponds to negligible chamber pressure relative to exit pressure required to drive the flow. Practically, however, there is an ignition process involving the spreading of the flame and some flow from the slots for which the orifice represents an obstruction. Since these factors can not be analyzed, the approach used here is to take C_v constant based on the data observed after the initial transient and to assume the same value applies during the start-up phase. The effect of the variable discharge coefficient is partly hidden in the form assumed for the burning rate during ignition.

In the spin fixture experiment, the gas generator exhausted into the atmosphere, and thus the exit pressure is sea level ambient for the assumed low speed injection. The exit density is assumed to be a function of the gas exit pressure, molecular weight and exit temperature. Since the speed is assumed to be low subsonic, there is relatively little kinetic energy in the gas and the exit temperature can be considered the same as the chamber stagnation temperature. Thus, it is concluded that all the factors in the following term are approximately constant after the initial transient in the laboratory tests:

$$K \equiv C_v A_e \sqrt{2\rho_e P_e}. \tag{9}$$

In the zero spin case, the regression rates are presumed to be the same on both surfaces since the chamber pressure history is basically monotonically decreasing with time.

Equation (8) shows that the the mass flow, $\dot{m}$, varies as $P_c/P_e - 1$. If this is considered combined with equation (7) for the production of mass from the burning propellant, then the observed zero-spin chamber pressure distribution can be used to determine the constant K. The test data,[5] at zero spin, results in a value of K of 0.189 kg/s. In these computations, the burning rates are assumed proportional to those measured by Miller. The strand burning rate is increased by a small constant factor, f_0, of 1.07 in order to obtain agreement with the ground based tests with zero spin. Taking into account the different conditions of the spin fixture and strand burning tests and the experimental accuracy, no significance is attached to the 7 per cent disagreement between the actual gas generator performance and the strand burning tests.

It should be noted here that there is an alternate explanation for the effect of spin on the pressure-time history. The burning rates could be a function of time or $r\Omega$, increasing and decreasing in such a way as to produce the chamber pressure variation. However, the regression rates of most homogeneous solid propellants are found to be only functions of pressure and initial propellant temperature and are independent of time except for an initial or final transient phase.

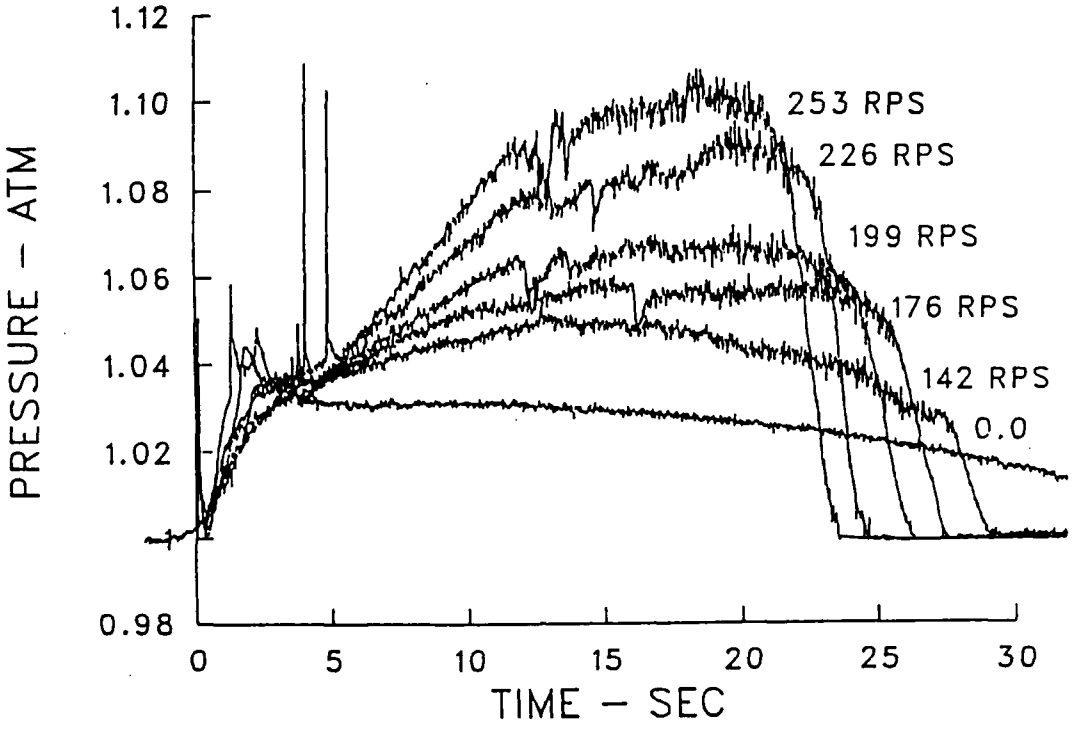

Figure 7: Effect of Spin on Chamber Pressure, AP-2 Propellant, (Ref. 5)

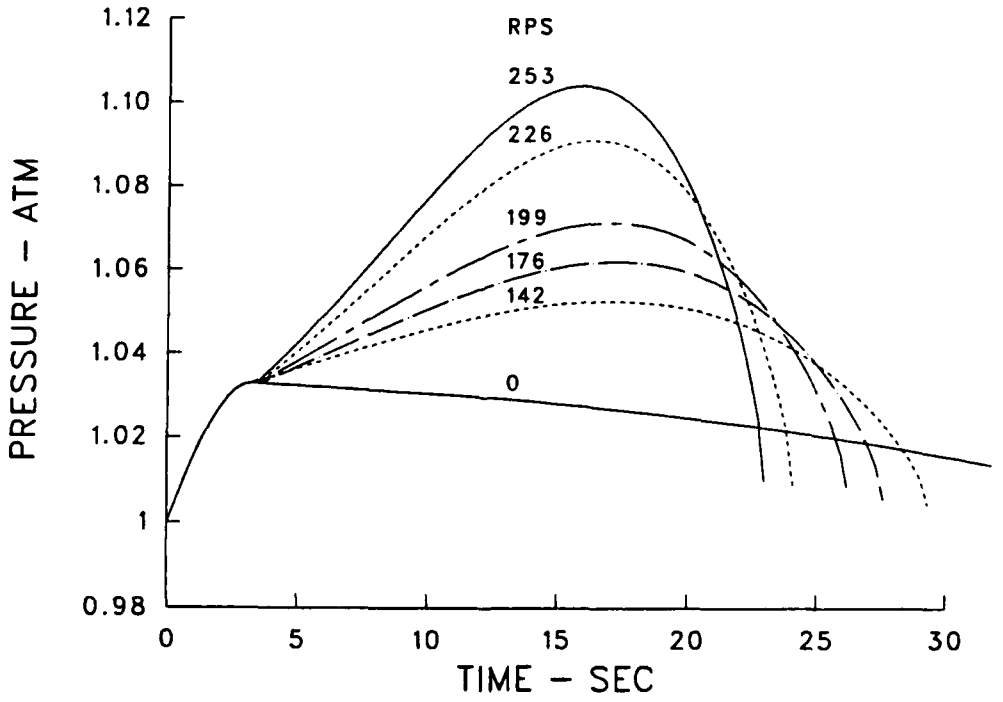

Figure 8: Computed Chamber Pressure Versus Time for Various Spin Rates.

2. EFFECT OF SPIN

In the following, provision is made for the possibility that the two propellant surfaces burn at different rates with spin,

$$\dot{r}_c = f_c(p)\dot{r}_0,$$

$$\dot{r}_s = f_s(p)\dot{r}_0,$$

where f_c and f_s are factors related to the rate of spin.

First, it is observed (see Figure 7) that there is an initial transient which is relatively independent of spin. The pressure is 3.3 per cent higher than ambient at 3.3 seconds after ignition for all spin rates. After that point, the chamber pressures diverge, depending on spin. The calculations were performed during the initial transient phase, $t \leq t_1$, assuming identical but time varying regression rates of,

$$\dot{r}_c = f_0\sqrt{\sin(\frac{\pi t}{2t_1})}\ \dot{r}_0,$$

$$\dot{r}_s = f_0\sqrt{\sin(\frac{\pi t}{2t_1})}\ \dot{r}_0.$$

The radial thickness of the grain is the smallest dimension; thus, it determines the overall burn-time. As a result, f_c can be determined as a function of spin rate from the measured burn times. The mass flow, equation (7), is integrated over time for the known amount of propellant using different f_c values until the calculated burn-time matches the measured time.

The slot contribution affects the magnitude of $\dot{m}$ but does not affect the burnout time as long as the value of f_s is not too large. Conditions at the end of the initial transient phase define the burning rate of the slots. A trial and error search at each spin rate with various values of f_s was performed until P_c=1.033 at t_1=3.3 seconds. This is equivalent to assuming that the mass flux from the gas generator is independent of spin at the end of the initial transient phase. If the magnitude of f_s is not selected consistent with this condition, then a discontinuous change in pressure is calculated at t_1.

Because the mass flow is constant at t_1, any increase in the cylindrical surface burning rate is matched by a corresponding decrease in the rate in the slots. Note that during the initial phase, the cylindrical and slot areas are about the same (see Figure 5). It is not clear what will happen at high spin rates if the flux from the slot goes to zero. Additional tests are needed in this range of spin rates which correspond to launch Mach numbers above 2.4.

The results are shown in Figure 8 where the predicted chamber pressure is plotted against time for the various spin rates of the spin fixture tests. This figure can be compared to Figure 7. Very good agreement is obtained during the early period when the effect of the different spin rates is being observed. At later times, there are some discrepancies which occur near the time when the curved surfaces, defined by r_s, affect the length of the grain.

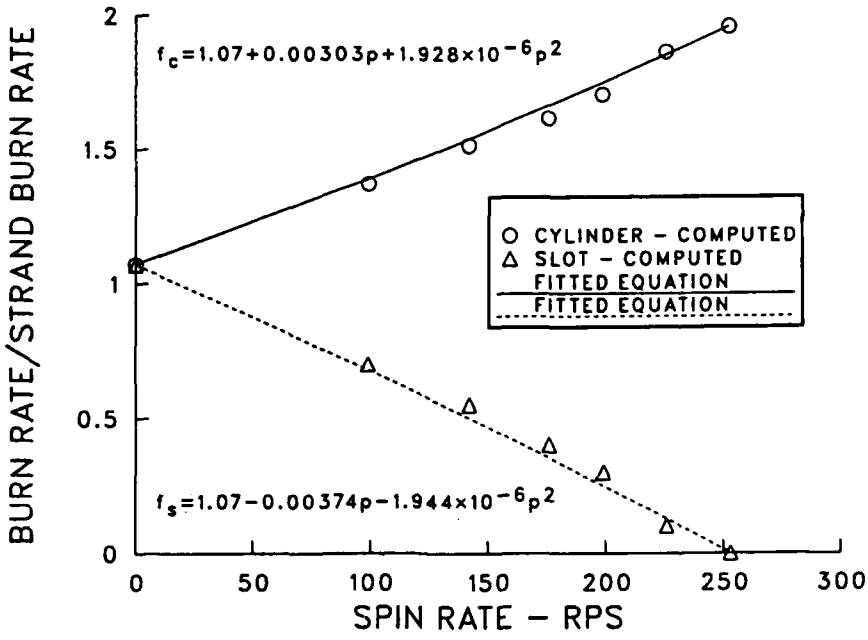

Figure 9: Effect of Spin Rate on Burn Rate for The Cylindrical and Slot Surfaces

The most important result, for subsequent calculations of the flight case, is the effect of spin on the burn rate. Figure 9 shows the spin factors, f_c and f_s, plotted versus the spin rate. Two empirical formulas that describe the spin rate effect are shown on the figure.

Comments:

1. The above results were obtained taking the ignition transient time of 3.3 seconds into account. Flight tests seem to indicate a shorter ignition transient delay probably because of the pre-conditioning of the propellant by the gun gases.

2. The dimensions r_{mx}, r_s and l_i as shown in Figure 3 were reduced by 1.0 mm (2.0 mm for l_i) to account for the inhibitor which coats the surfaces adjacent to the motor case. The coating prevents combustion on these surfaces. The specifications for the propellant call for an inhibitor thickness from 0.5 to 1.3 mm.

3. APPLICATION TO FLIGHT TESTS

In applying the above analysis to the flight situation, it is assumed that the exit pressure, P_e, becomes the base pressure, P_b, thus:

$$K_{flight} = K \frac{P_\infty}{P_{sl}} \frac{P_b}{P_\infty},$$

and

$$\dot{m} = K\frac{P_\infty}{P_{sl}}\frac{P_b}{P_\infty}\sqrt{\frac{P_c/P_\infty}{P_b/P_\infty} - 1}. \tag{10}$$

The above formula is based on assuming incompressible flow, which is correct if the ambient pressure is high as it is in the ground based tests. A more general formula applicable to compressible flow in the gas generator can be written as:

$$\dot{m} = K\frac{P_c}{P_{sl}}\left(\frac{P_b}{P_c}\right)\sqrt{\frac{\gamma_g}{(\gamma_g - 1)}\left[\left(\frac{P_c}{P_b}\right)^{\frac{\gamma_g - 1}{\gamma_g}} - 1\right]}. \tag{11}$$

Note that the magnitude of γ_g is unimportant except when the exit velocity is close to

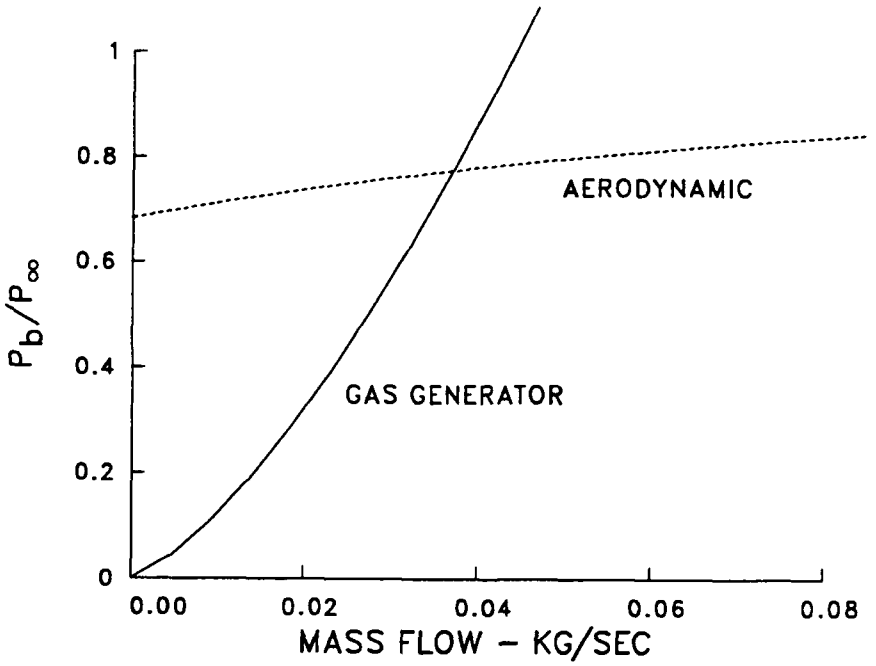

Figure 10: Sketch of The Solution Technique

conditions which choke the exit. A value of 1.25 has tenatively been assumed. If the pressure ratio P_c/P_b becomes large enough, the exit Mach number becomes sonic and the pressure ratio appearing in equation (11) can be written:

$$\left(\frac{P_c}{P_b}\right)_{max} = \left(\frac{2}{\gamma_g + 1}\right)^{-\frac{\gamma_g}{\gamma_g - 1}}. \tag{12}$$

If the flow chokes because of a low base pressure and the resistance of the orifice, which can occur at high launch Mach number or high altitude, consideration should be given to the variation of the discharge coefficient (i.e., K). The result is to increase the discharge

coefficient[33,34] in the range of 10 to 40 per cent as the pressure ratio, P_c/P_b, increases to 5.0 after which the C_v remains constant. In this report the focus is on low injection rates and therefore C_v is take as constant.

The mass flow generation formula, equation (7), remains the same: Equations, (7) and either (10) or (11), may be considered, at each point in time, as two equations with four unknowns, $\dot{m}$, P_b/P_∞, P_c/P_∞, P_∞/P_{sl}. At a point along the trajectory M_∞, and P_∞/P_{sl} would be known, and aerodynamic theory gives a third relation between $\dot{m}$ and P_b/P_{sl} (also involving M_∞ and P_∞/P_{sl}) which determines the solution at each point in time. Figure 10 sketches the solution technique.

4. IGNITER

The solid propellant fuel is relatively difficult to ignite and, therefore, the gun gases are supplemented by an independent igniter. This consist of two 6.2 gram cylindrical pellets of magnesium-teflon, see Figure 2. It has been estimated that this material is consumed in approximately two seconds. At that rate and considering the high temperature of these gases, the igniter contributes significantly to the flow from the device in the first seconds of flight. The temperature of the the igniter products is estimated at 3000 K. It is assumed that there is a linear build-up of mass flow for 0.25 seconds followed by a constant flow of igniter material until it is consumed. In computing the injection parameter, I, the igniter mass flow is added to that of the main propellant. The temperature of the exhaust is estimated as the mass average for the purposes of determining the slope of the base pressure as will be discussed in the next section.

IV. AERODYNAMICS OF BASE INJECTION

It is customary when considering base bleed or burn to define a nondimensional injection parameter, I:

$$I = \frac{\dot{m}}{\rho_\infty u_\infty A_{ref}} \tag{13}$$

In the M864 case, the average value of this parameter is,

$$I = \frac{0.00432}{M_\infty(\rho_\infty/\rho_{sl})},$$

(assuming a fuel mass=1.21 kg and a burn time=33.0 seconds). Thus, it is concluded that a typical value for I at launch is about 0.002 and that I increases as the Mach number decreases and as the altitude increases. Note that the most significant potential drag reduction occurs during the early, supersonic phase of flight.

It is possible that I, the injection parameter as defined above, is not the appropriate parameter with which to correlate these results. A nondimensional injection parameter based on the momentum flow in the attached boundary layer before separation has been suggested by Collins, et al[35] as being more representative of the free shear layer characteristics. One can also speculate that the base pressure is affected by an increase in the

volume of the wake as a result of two effects. First, there is the direct effect of volume of the added mass, and second, there is the effect of heating the wake air. Thus a volume injection parameter coupled with a separate temperature parameter might be more logical from a physical point of view. Never-the-less, the authors of the existing literature have generally used the mass flow definition of I.

1. BACKGROUND REVIEW

Most supersonic wind tunnel experiments on this subject are concerned with cold gas injection into the base region at relatively large values of I. Figure 11 shows the results of one such experiment by Kayser.[20] In this test he investigated the effect of the injector geometry (i.e, per cent open area of the base) on the base pressure. The results are for a Mach number of 3.0 with cold air injected into the model wake. Note that there is a strong dependence on injector open area at large values of I. However, all the curves originate at the same pressure and increase linearly at the same slope for values of I less than about 0.005. This suggests that, at small injection rates, a linear increase in base pressure can be assumed, although as the injection rate gets larger such an approximation may overestimate the beneficial effects. Similar results regarding the effect of injector geometry have been reported by Reid and Hasting.[38]

Figure 12 shows the effect of Mach number on the base pressure versus injection rate curves.[36] These results show that at low values of I, the pressure again increases linearly but that the slope of the curves decrease with decreasing Mach number. Furthermore, the maximum in the curves occurs at larger I at the lower Mach numbers. This is fortunate because the average I increases with decreasing Mach number.

Figure 13 shows another experiment of Clayden and Bowman,[37] in which high temperature argon was injected from a model base into a Mach number 2.0 wind tunnel air stream. The injection rate is much less in these experiments because, at equal mass flow rates, the injection velocity is greatly increased as the temperature increases. At low injection rates, the data can also be represented by a linear increase in base pressure with I. At higher temperatures, the curves are more nonlinear; but this may be beyond the range of interest for the M864.

2. LINEAR EFFECT OF INJECTION ON BASE PRESSURE

As a preliminary approach, it is assumed that the mass injection rate is at sufficiently low subsonic velocities that the injection effect on base pressure is nearly linear, i.e.,

$$\frac{P_b}{P_\infty} = \left(\frac{P_b}{P_\infty}\right)_{I=0} + \left[\frac{d(P_b/P_\infty)}{dI}\right]_{I=0} I. \tag{14}$$

A number of reports on wind tunnel measurements of base pressure with injection have been examined. Figure 14 shows the results of determining $[\frac{d(P_b/P_\infty)}{dI}]_{I=0}$ as a function of the free stream Mach number. The open symbols represent wind tunnel experiments in which

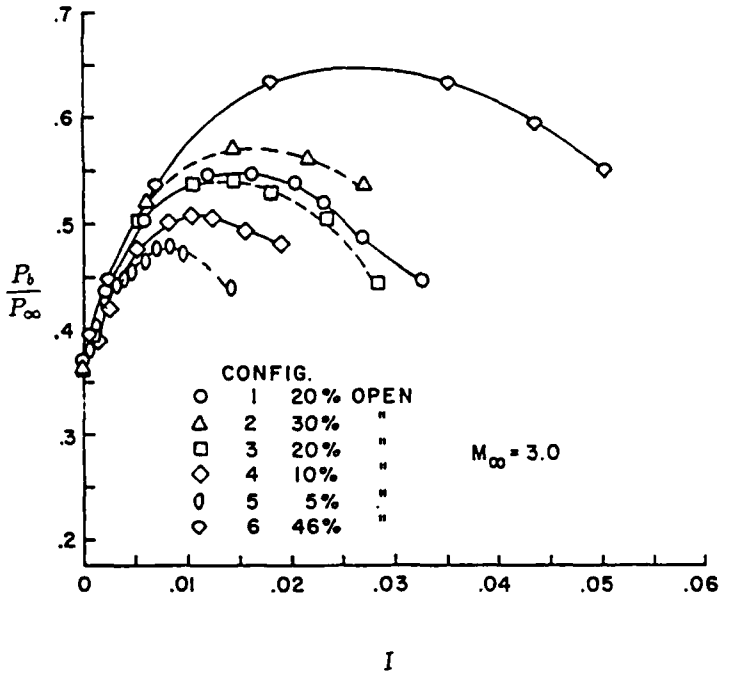

Figure 11: Effect of Injector Open Area on Curves of Base Pressure Versus Injection Rate, (Ref. 20)

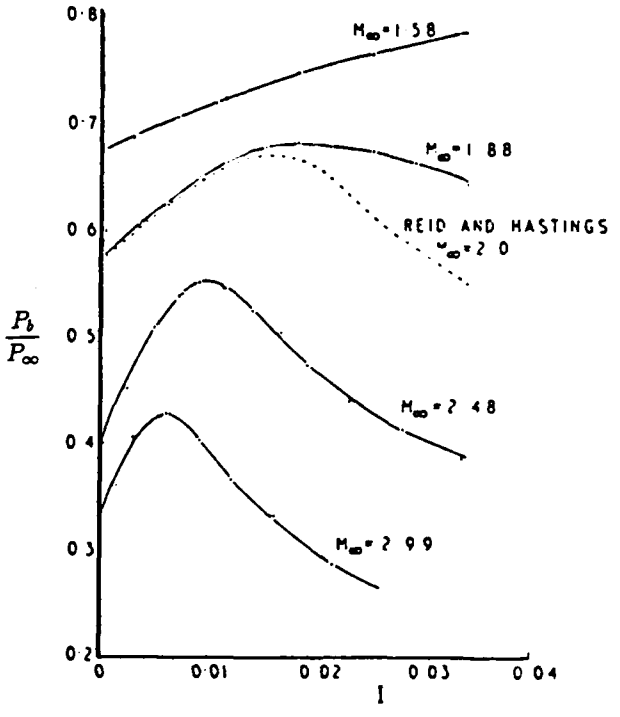

Figure 12: Effect of Mach Number on Curves of Base Pressure Versus Injection Rate, (Ref. 36)

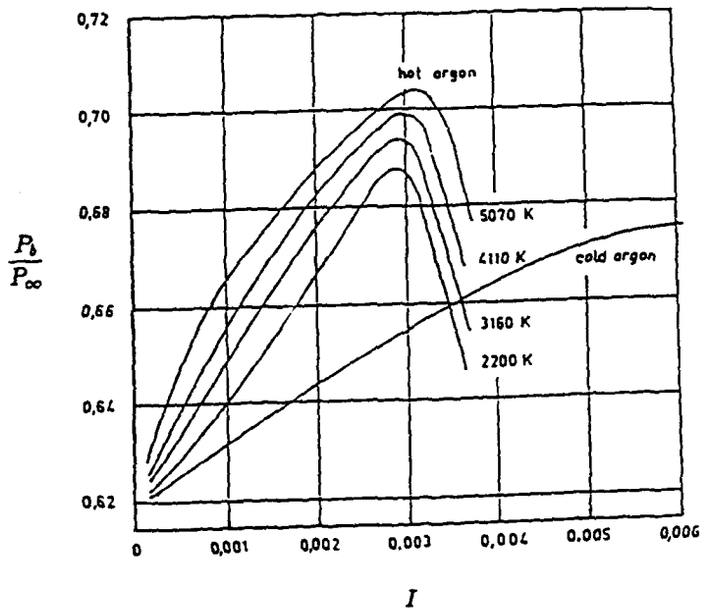

Figure 13: Effect of Gas Temperature on Base Pressure at M_∞=2.0, (Ref. 37)

ambient room temperature air was injected. Although these data correlate reasonably well with Mach number, they represent a special case of low temperature injection into a low temperature wake (stagnation temperature of the wind tunnel flow is estimated also to be ambient room temperature.)

Relatively little is known about injection at transonic and subsonic Mach numbers. The computational data of Sahu[8] and the experimental data of Sykes[39] have been used in Figure 14.

Also included in Figure 14 are three points (filled symbols) computed by Nietubicz.[40] The magnitude of the numerical results agree quite well with the wind tunnel data. There is possibly some difference in the trend of the computed results; but, as will be discussed, the conditions in terms of the Reynolds number and stagnation temperature of the free-stream flow are quite different.

Other numerical computations[8,41] of the near wake flow with injection have become available to broaden our data base for these kinds of flows. These computations involve solution of the perfect gas Navier-Stokes equations. Both the free-stream and injected gas are air. The stagnation temperature of the injected gases was selected to provide one of the boundary conditions on the exit plane of the injector. The solution is marched in time until the flow converges to steady state. The computed base pressures were integrated over the base area to determine the total base drag. An average base pressure was then calculated from the computed drag. The computations have been performed using the actual M864 base geometry which includes an indented and domed configuration. The free-stream

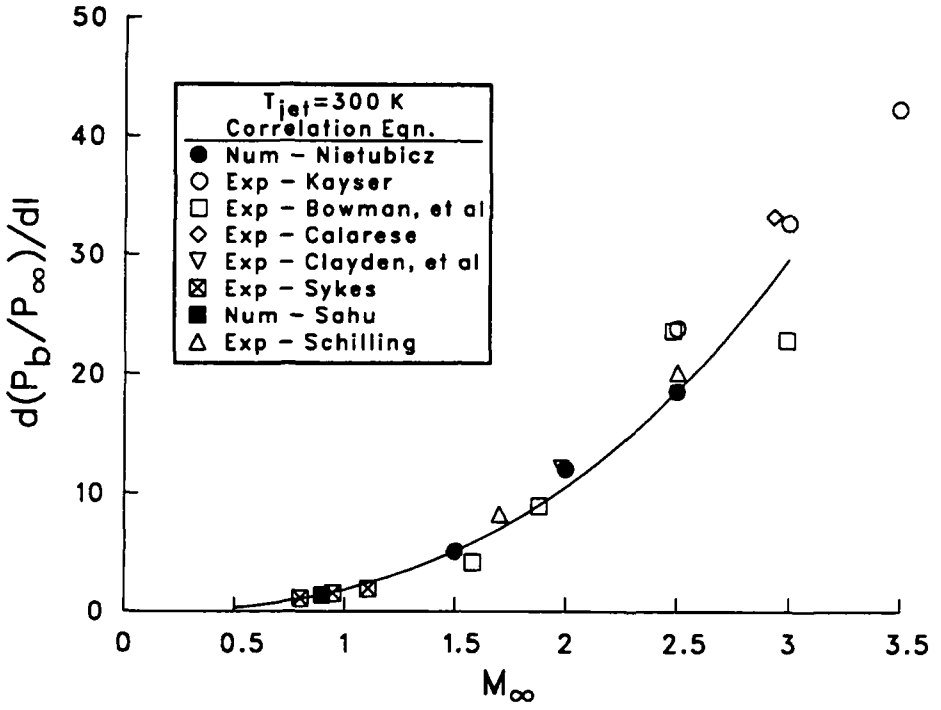

Figure 14: Slope of Base Pressure Curve Versus Mach Number at Low Injection Temperatures

boundary conditions correspond to the flight case at sea level standard conditions (as distinguished from the wind tunnel simulations).

The results of these computations, in terms of the linear effect of injection, are shown in Figure 15. The data are unique in that they illustrate the combined effect of Mach number and injected gas temperature. The computed data at an injection temperature of 1500 K are consistent with the only data available.[42] At all stagnation temperatures of the gas, the slope $[\frac{d(P_b/P_\infty)}{dI})_{I=0}$ increases rapidly with Mach number and almost linearly with temperature. An approximate formula which describes the data is:

$$\begin{aligned}[\frac{d(P_b/P_\infty)}{dI}]_{I=0} &= (-5.3953 + 0.01723T_j)M_\infty \\ &\quad +(4.6101 - 0.01463T_j)M_\infty^2 \\ &\quad +(-0.5660 + 0.00446T_j)M_\infty^3. \end{aligned} \tag{15}$$

Note that with this linear model (Equation 14) of the effect of injection on base pressure, it is possible to correct the no injection base drag to account for base bleed. At each step in a trajectory calculation where an estimate of Mach number, free-stream static pressure, spin rate and inert (no injection) drag coefficients are specified, then equations 7, 11, and 14, or a non-linear version to be discussed, can be solved simultaneously to find the change in base pressure with injection.

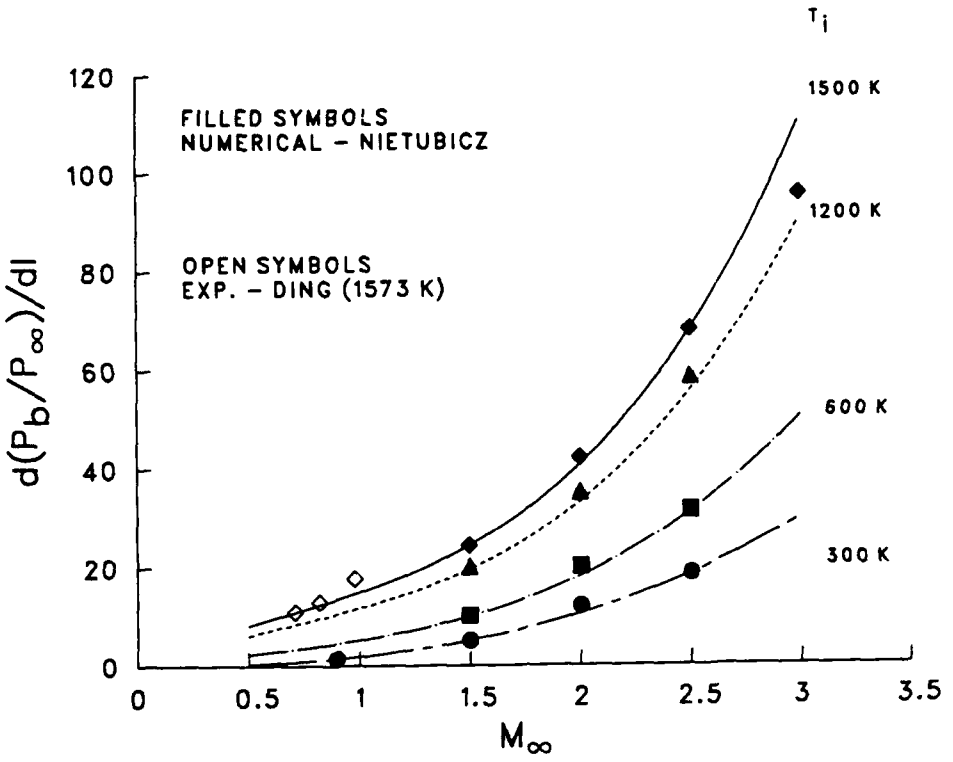

Figure 15: Slope of Base Pressure Curve Versus Mach Number at High Temperature

3. NON-LINEAR EFFECT OF INJECTION ON BASE PRESSURE

It is apparent, even at low injection rates, that the effect on the base pressure is non-linear. At subsonic speeds the nonlinearity can not be ignored because the low speed base pressure curves appear to asymptote to constant values slightly higher than free-stream static pressure at large values of I. As a strictly curve fitting technique, the following form has been assumed:

$$\frac{P_b}{P_\infty} = \left(\frac{P_b}{P_\infty}\right)_{I=0} + \frac{\sigma I}{(1+\beta\sigma I)} \tag{16}$$

σ equals the slope $\frac{d(P_b/P_\infty)}{dI}$ and the parameter β determines the importance of the non-linearity. It has been found to be just a function of Mach number as follows

$$\beta = 15.1 - 46.3(M_\infty - 0.71)$$

but not less than β=2.6 . Figure 16 shows the resulting base pressures versus injection rate, I, for a range of Mach numbers from subsonic to 2.5. The curves have been computed from the correlation equations. Also shown on the graph are the numerical data of Nietubicz and the experimental data of Ding. The agreement is reasonably good. The predicted lines originate at values of the base pressure computed from an estimate of the base drag which will be discussed later. The disagreement between the lines and the numerical results is due to disagreement in the computed base drag relative to experimental data.

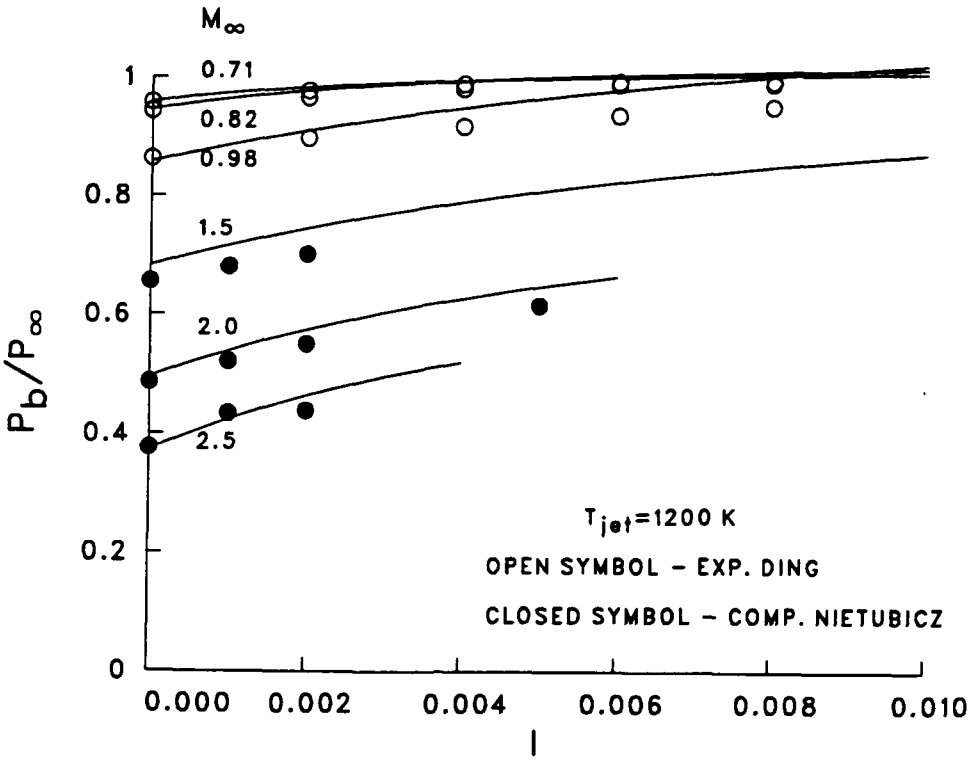

Figure 16: Computed Base Pressure Versus Injection Rate Compared to Numerical and Experimental Data

4. BASE BURN

It is apparent in observing the flight of M864 projectiles that the products of combustion produce considerable illumination in the near wake region.[3] This suggests that the gas products in the base region are fuel rich and react with the oxygen in the base region air. The studies that have been performed on base region combustion[27,43] have shown that there can be a significant effect on base pressure. Most of these studies have employed reactive gases such as hydrogen. Partial preburning of the injected reactant can even be beneficial because the base pressure is produced by a combined effect of direct volume addition to the near wake, and expansion of the wake because of the mixing of hot gases and heat release through reaction. It is not clear, at this time, how the wake combustion for the M864 propellant can be modeled. Tentatively, it is assumed that the injected gases should be considered to have an effective stagnation temperature different from the combustion chamber temperature. The increase in the effective T_c is assumed to produce the same effect as the energy release in the wake. This feature has been incorporated into the current model. However, data are lacking on the M864 propellant with which to analytically estimate this effective stagnation temperature. Even the ground base measurements of chamber temperature are suspect because of the significant amount of contamination found on the thermocouple after the tests. These tests indicated a chamber temperature of roughly 1200 K. Subsequent flight tests in which similar measurements were made indicated a higher temperature of 1500 K. Ding et al[42]used a solid propellant with a burning temperature of 1573 K in a low speed wind tunnel test, as previously

discussed. Their results were consistent with extrapolation of the supersonic numerical calculations of air injected at 1500 K.[40] In the calculations reported here, the temperature of the combustion products has been taken to be 1500 K and no account has been taken of the external burning.

V. TRAJECTORY

A simple two degree of freedom, point mass trajectory computation has been coupled with the equations defined above to perform a complete analysis.

1. TWO-DIMENSIONAL TRAJECTORY MODEL

A fourth order Runga-Kutta integration is performed on the two second order momentum equations and a first order spin equation (where x corresponds to range direction and y to height). The equations solved are:

$$\frac{d^2x}{dt^2} = f_x, \tag{17}$$

$$\frac{d^2y}{dt^2} = -g + f_y, \tag{18}$$

$$\frac{dp}{dt} = f_p, \tag{19}$$

where;

$$f_x = -C_D \frac{1}{2} \rho_\infty u V A/m, \tag{20}$$

$$f_y = -C_D \frac{1}{2} \rho_\infty v V A/m, \tag{21}$$

$$f_p = C_{l_p} \frac{1}{2} \rho_\infty V p D^2 A/I_x. \tag{22}$$

In order to obtain an accurate evaluation of the range of the projectile, account has to be taken of the Magnus forces acting on the spinning body. Although the trajectory is entirely two dimensional, a yaw of repose is calculated to account for the effect of the curved trajectory on the spinning body. This yaw is a balance between the gyroscopic moment produced by the curved flight path and the aerodynamic moment. It can be computed from:

$$\alpha_e = -\frac{2I_x p(u\dot{v} - v\dot{u})}{\rho_\infty A D C_{M_\alpha} V^4}. \tag{23}$$

The acceleration components in the x and y directions produced by the Magnus force, which acts perpendicular to the velocity vector, are added to the f_x and f_y as:

$$(x - component) = +C_{Y_{p\alpha}} \frac{1}{4} \rho_\infty A D p(\alpha_e v)/m, \tag{24}$$

and

$$(y - component) = -C_{Y_{pa}} \frac{1}{4} \rho_\infty A D p (\alpha_e u)/m. \tag{25}$$

A secondary effect of the yaw of repose is a contribution to the drag coefficient which is proportional to the square of the yaw angle.

Finally, the curvature of the earth is accounted for at each step by adding to the altitude change computed from the vertical component of acceleration, the quantity:

$$(curved\ earth\ contribution\ to\ y) = \frac{(x_- + \Delta x)^2 - x_-^2}{2\ R_{earth}}.$$

Where x_- is the range at the beginning of the time step and Δx is the change in range computed from the acceleration.

2. AERODYNAMIC COEFFICIENTS

At each step of the calculation, a subroutine is called to define the standard atmosphere free-stream density, pressure and velocity of sound as a function of the local altitude. A standard polynomial representation is used. A second routine computes the inert round's zero-yaw drag coefficient as well as the spin damping and other aerodynamic properties of the basic shell. This routine uses a spline interpolation technique based on tabulated data (see Table 2) to determine these quantities as a function of free-stream Mach number. The overall drag data are based on measurements obtained in the BRL Transonic Range[44] and from radar data obtained in flight tests.[6] The Navier-Stokes computations of the M864 forebody pressure and friction drag,[45] also given in Table 2, have been subtracted from the total inert drag to determine the base drag coefficient, i.e.:

$$C_{D_{b_\bullet}} = C_{D_\bullet} - C_{D_{pv}}. \tag{26}$$

Average base pressure is then computed from the base drag,

$$\frac{P_{b_\bullet}}{P_\infty} = 1 - \frac{\gamma}{2} M_\infty^2 \frac{A_{ref}}{A_b} C_{D_{b_\bullet}}. \tag{27}$$

Figure 17 illustrates drag coefficient data used in these computations. Note that Figure 17 also includes the Navier-Stokes computations of Nietubicz.[40] The base drag coefficients at supersonic speeds are obtained directly, in this case, by solution of the fluid dynamics equations for the actual base geometry. The agreement with the experimentally determined $C_{D_\bullet}$ curves is generally good.

Once the inert aerodynamic properties have been determined, the subroutines which compute the gas generator-on aerodynamics are invoked. This section of the code computes the mass flow, base pressure and gas generator chamber pressure, using iteration, starting with an initial estimate of the base pressure. The equations developed in the section on the gas generator and the bleed aerodynamics are solved. When the base pressure with

TABLE 2: INERT M864 AERODYNAMIC CHARACTERISTICS

M_∞	C_{D_o}	$C_{D_{pv}}$	C_{M_α}	C_{l_p}
0.00			4.32	-0.0178
0.50				-0.0145
0.70	0.168	0.0600		
0.80	0.163	0.0569	4.32	
0.90	0.175	0.0579	4.60	
0.92	0.185			
0.94	0.205			
0.95		0.0817		
0.98	0.285	0.0921		
1.00	0.335			-0.0123
1.01		0.1162		
1.05		0.1420		
1.08	0.350			
1.10	0.348	0.1421		
1.15	0.342			
1.20		0.1364		
1.25	0.330			
1.30		0.1308		
1.40			4.70	
1.50	0.302	0.1181		
1.75	0.280			
2.00	0.262	0.1009		-0.0096
2.50	0.234	0.0950	4.70	-0.00875

NOTES:

1. C_{D_o} is based on transonic range data[44] for $M_\infty \leq 1.10$ and on radar flight data[6] for $M_\infty > 1.10$.

2. $C_{D_{pv}}$ is the sum of numerically computed forebody pressure and viscous drag coefficients obtained by Sahu.[45]

3. Additional constant aerodynamic parameters used in the trajectory calculation are: $C_{D_{\alpha^2}} = 7.2$ and $C_{Y_{p\alpha}} = -3.20$.

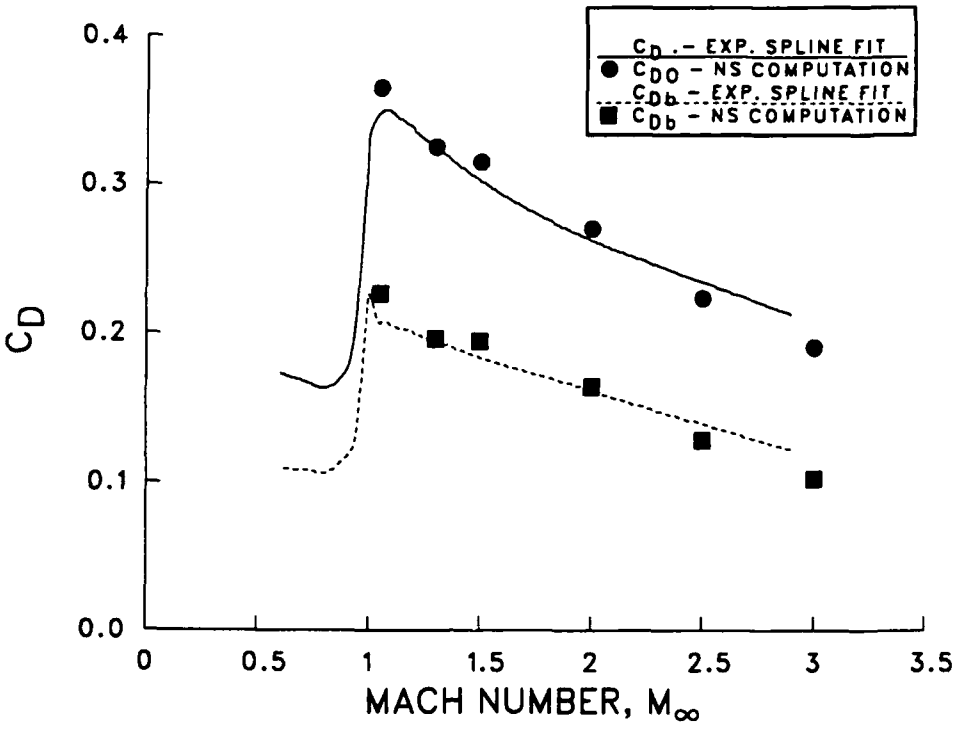

Figure 17: Zero Yaw Total and Base Drag Coefficients Versus Mach Number for the Inert M864

base bleed is determined a local drag reduction factor, f_{dr}, is computed:

$$f_{dr} = \frac{\frac{P_b}{P_\infty} - \frac{P_{b_o}}{P_\infty}}{1 - \frac{P_{b_o}}{P_\infty}}. \tag{28}$$

The drag reduction factor is passed to the Runga-Kutta integration and used to compute the reduced drag coefficient as follows:

$$C_D = C_{D_o} - f_{dr} C_{D_{b_o}}. \tag{29}$$

In addition to the drag reduction factor, the mass of consumed fuel is computed so that instantaneous mass is used in the equations.

3. VALIDATION OF TRAJECTORY MODEL

The trajectory computations were checked by comparison with the trajectories computed by a full three-dimensional point mass technique[46,47] for a range of launch conditions. The results for the inert M864 are shown in Figure 18. The total range is in agreement with the more complete method within 60 m at 24,000 m or less than 0.25 per cent. Another check of the inert calculation is to compare the spin history from the two techniques as shown in Figure 19. The agreement is again excellent. The final spin being computed within 0.5 per cent.

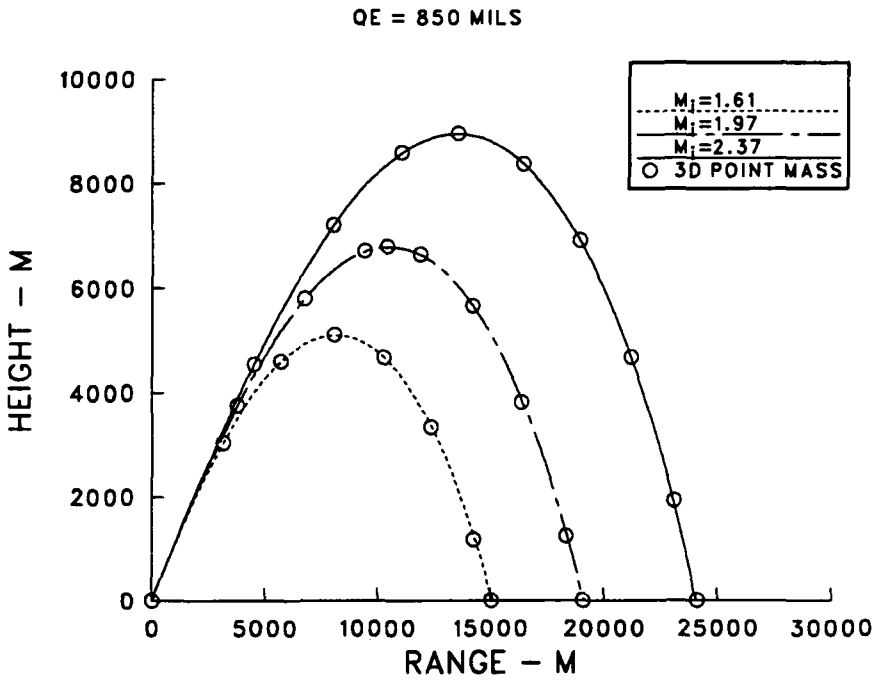

Figure 18: Comparison of 2D Trajectory Computations with 3D Modified Point Mass Trajectory.

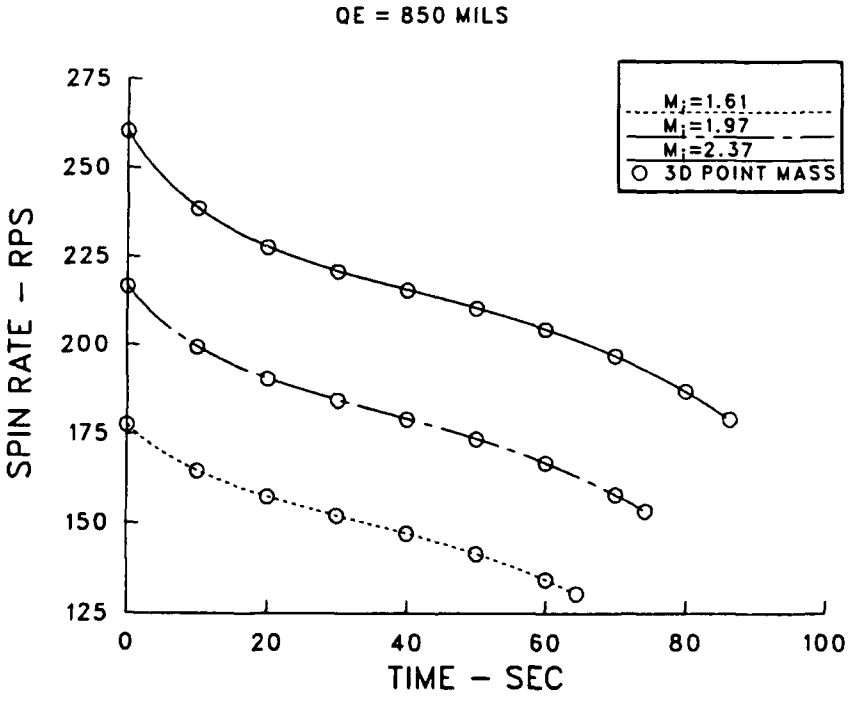

Figure 19: Comparison of 2D Computed Spin Rate with 3D Modified Point Mass Predictions.

VI. RESULTS

The theory developed in the previous three sections has been programmed for the BRL Vax 8600 computer and the technique compared to several flight test cases. The primary case is that of an instrumented M864 flight [48] in which the base and combustion chamber pressures were measured in flight. Radar flight data also have been obtained by Lieske[6] over a range of launch conditions. These data have been used to formulate an empirical prediction technique which computes the trajectory for the purpose of generating firing tables. These results are compared to the present model's predictions.

1. INSTRUMENTED FLIGHT TEST CASE

Kayser, et al[48] launched an instrumented M864 in September 1988. The projectile contained pressure transducers to monitor the static pressure at two points on the base and the stagnation pressure in the combustion chamber. In addition, a thermocouple measured the temperature in the combustion chamber. Pressures on the ogival nose were also measured. These data were telemetered to recording stations on the ground. A yawsonde helped define the epicyclic motion during part of the flight and radar tracked the trajectory. The projectile was not a standard M864 in that the mass was 81.9 per cent of normal. The launch conditions, Mach 1.30 at a quadrant elevation of 850 mills, did not correspond to standard operating conditions and were selected in order to optimize the chances of a successful initial test flight of the instrumented round.

Figure 20 shows a comparison between the predicted trajectory for this round with the motor on and with motor off. The effect of drag reduction caused by the gas generator results in a 23 per cent increase in range. Unfortunately, the radar tracking did not cover the entire trajectory to impact. Thus, experimental data are unavailable for a direct comparison with these computations.

Figure 21 shows the predicted spin rate compared to the flight measurement of spin rate using the onboard yawsonde. The prediction is initially in good agreement with the data but tends to over predict spin by less than one per cent at 20 seconds. This disagreement can be related to a small change in the roll damping coefficient. However, for the computation of the burn rate as a function spin, this discrepancy is negligible.

Figure 22 shows the main result of the experiment which is the pressure-time histories for two points on the base and in the chamber. The origin of the time scale is with respect to the exit of the shell from the gun. The initial base pressure corresponds to the inert projectile at Mach number of 1.30 . The chamber pressure port was deliberately sealed with a combustible material. As a result, the chamber pressure sensor did not begin to detect the gas pressure until approximately 5 seconds after shot exit. The position of the port was in the slot between the grains. Delay in recording may have been caused, in part, by distortion in the grain blocking the slot. This is suspected because of the rather unexpectedly large delay.

The two base pressure taps indicated almost the same pressure throughout the burning

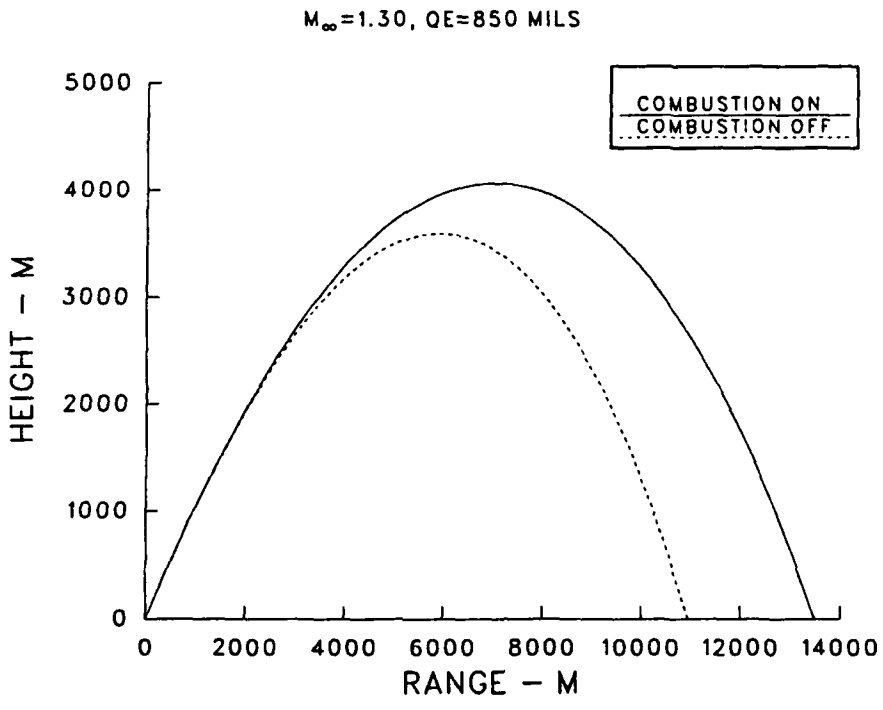

Figure 20: Predicted Trajectory for M864-L Flight With and Without Burn

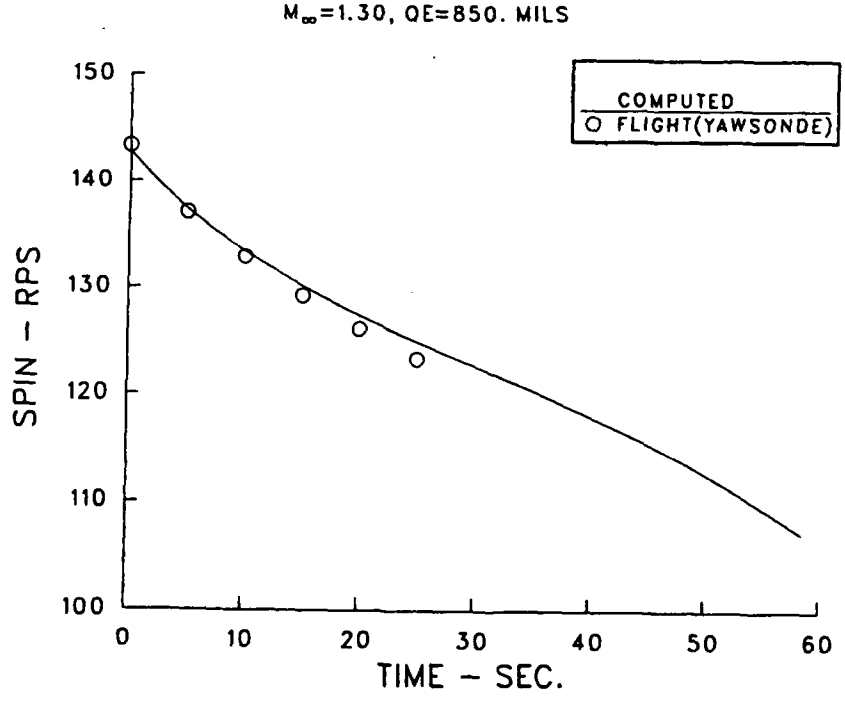

Figure 21: Comparison of Predicted Spin Rate for The M864-L Flight with Yawsonde Measurements

phase, although there was a significant difference after burnout. These pressures initially increased to a peak of 0.89; the pressure then followed the expected variation with local atmospheric pressure. The only major exception is a jump as the projectile decelerates through Mach number one at 8. to 9. seconds into the flight.

The chamber pressure measurements roughly parallel the base pressures but at a some what higher level as needed to produce the gas generator exhaust. The ratio of the two pressures indicates that the flow through the exit is subsonic throughout the burn. The chamber pressure drops to that of the base flat at 35.3 seconds. This is an indication of the actual burnout time, although the two base pressure measurements show an altered behavior well ahead of the apparent burnout. This suggests that the wake sensed a weakening motor output well before the chamber pressure completely dropped to the level of the base.

The next figure, 23, shows the computed pressure histories using the present analysis. The results are in resonably good accord with the previous experimental data. There are some discrepancies including that the base pressure did not jump up as high initially. This would seem to indicate that the initial drag reduction is not as great as obtained in flight. Never-the-less, the base static pressure decreased to a somewhat lower value corresponding to the projectile reaching an even higher altitude. A third line on this figure indicates the local ambient static pressure along the trajectory. The base pressure actually becomes larger than the local static indicating a thrust is being generated near the apogee. It should be pointed out that a standard atmospheric model has been used in the calculations rather than the measured atmosphere.

The chamber pressure history also roughly parallels the base pressure. The burnout is clearly observed at 36.8 seconds.

The next two Figures, 24 and 25, show essentially the same information as in the previous two except that all the pressures are divided by the free-stream static pressure. The static pressure is plotted in atmospheres for reference. In both the computed data (24) and measured data (25), the base pressure ratio in the subsonic flight (time greater than 10. sec.) is slightly greater than one. Thus, relative to free-stream ambient pressure, the base actually contributes a negative drag or thrust. In the same region the chamber pressure is about 6 to 8 per cent higher than the base pressure which is a sufficiently low ratio to assure subsonic ejection.

In the supersonic flight, there are a number of discrepancies such as the fact that the igniter contribution is over estimated and that the timing of the igniter activation is inaccurately modeled in detail. It is difficult to predict the igniter performance a priori without more specific data.

Figure 26 shows the drag reduction factor, f_{dr}, which is defined in equation (28) in terms of the base pressures with and without burn. The computation shows that base bleed reduces base drag about 50 per cent in the supersonic part of the flight and basically eliminates the base drag in the subsonic regime. The burnout occurs very abruptly because the uniform burning surface is modeled with significant size at the maximum diameter of the grain. In the experiment, irregularities probably cause the grain to burn through unevenly with a more gradual burnout.

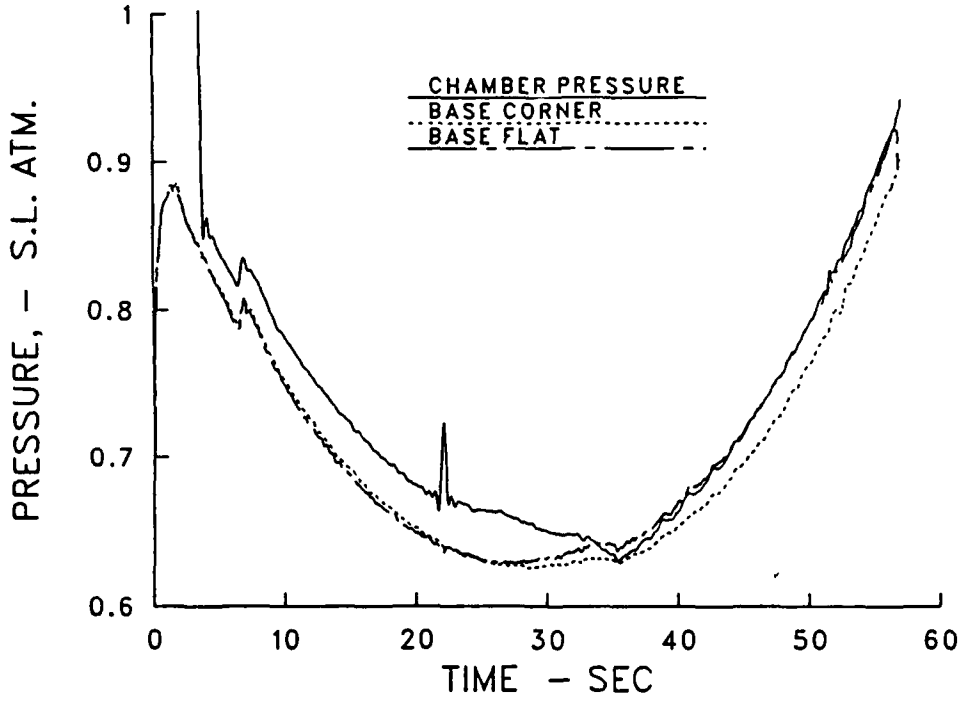

Figure 22: Experimental Chamber and Base Pressures Versus Time from M864-L Flight

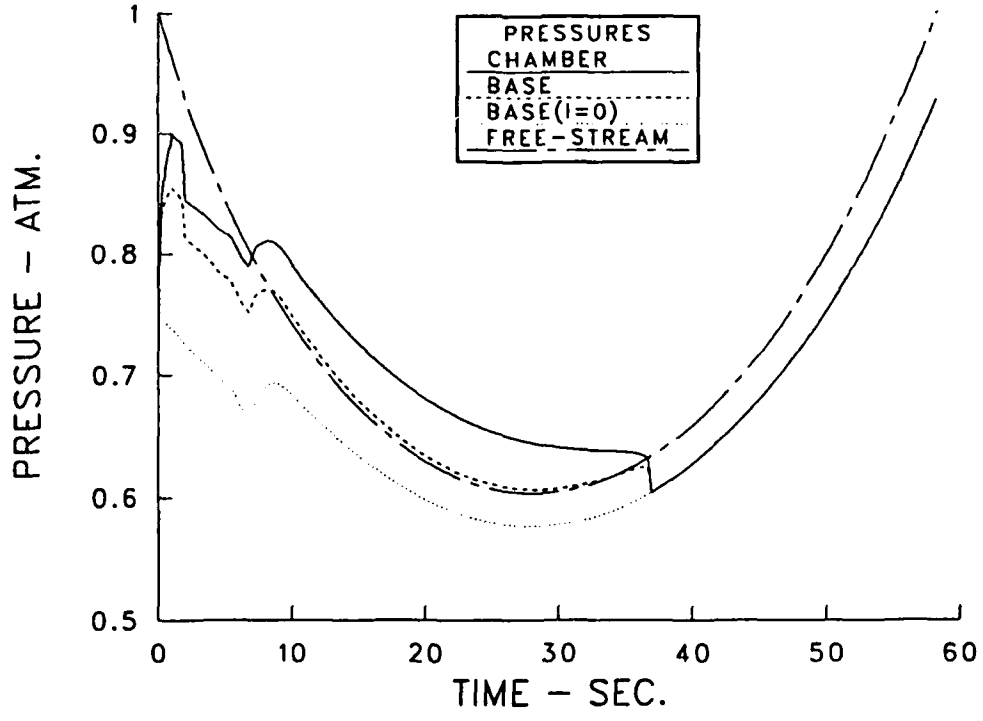

Figure 23: Computed Pressure Versus Time for M864-L Flight

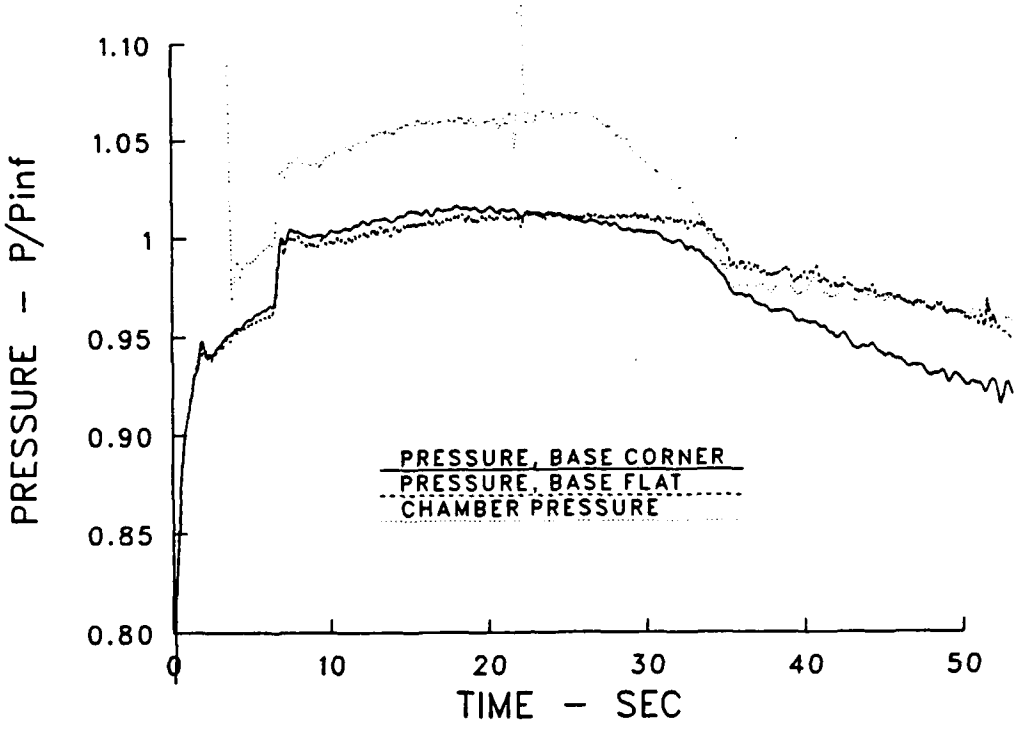

Figure 24: Experimental Chamber and Base Pressures Relative to P_∞ for The M864-L Flight

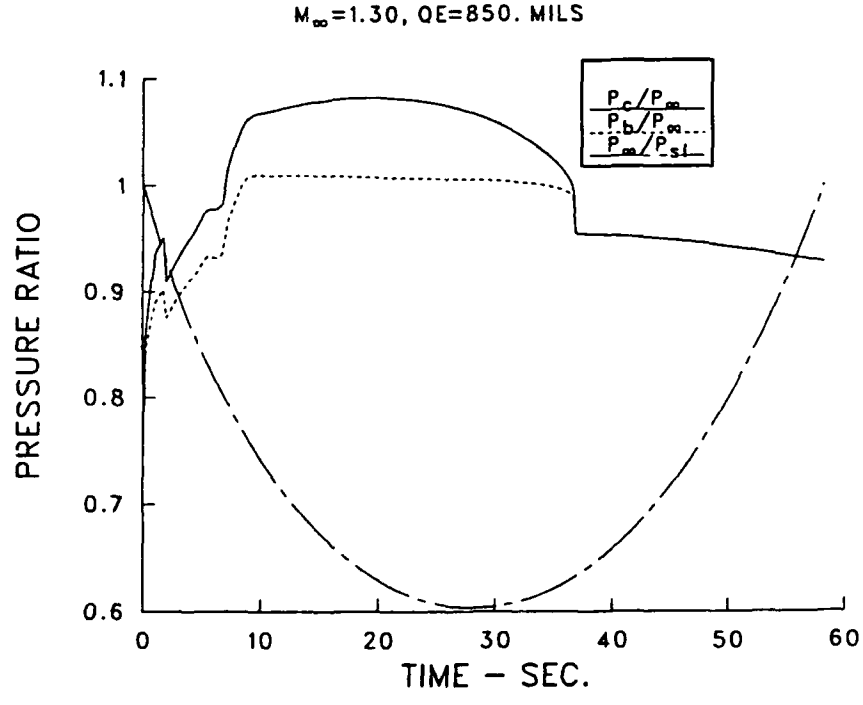

Figure 25: Computed Pressure Ratios for the M864-L Flight

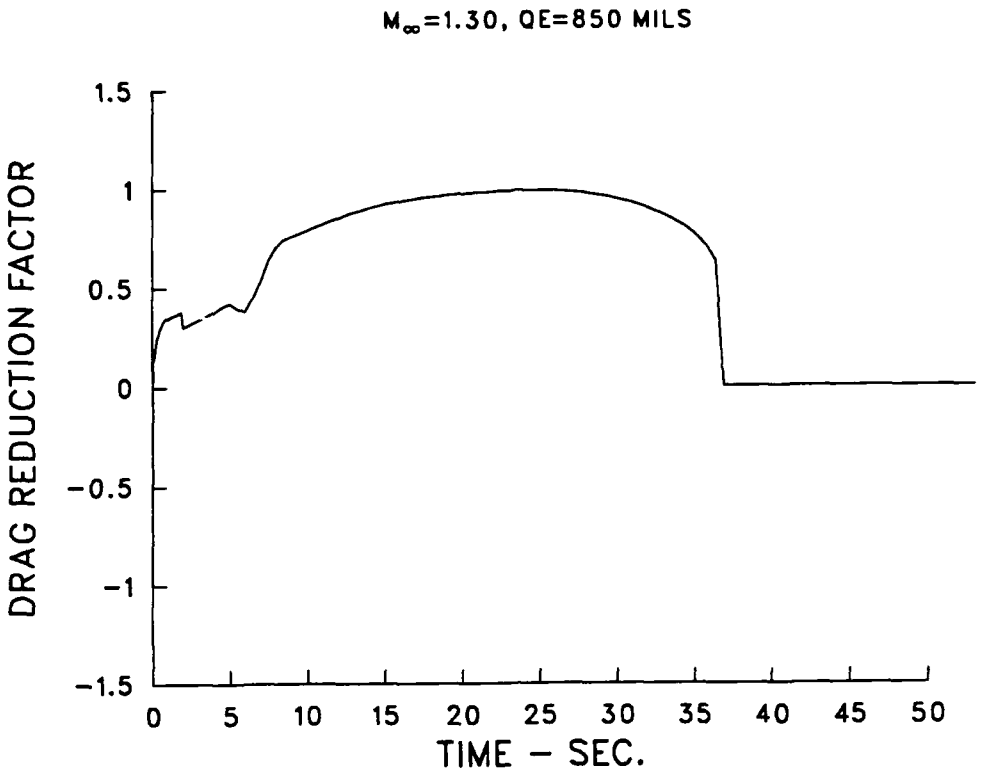

Figure 26: Drag Reduction Factor for M864-L Flight

The mass flow from the gas generator is shown in Figure 27. Except for the pulse from the igniter, the mass flow from the generator is between 0.030 and 0.034 kg/s over 75 per cent of the burn time.

2. COMPARISON WITH FIRING TABLE DATA

In order to develop firing information for the M864, the Firing Tables Branch of the Launch and Fight Division of BRL has been conducting flight tests of production ammunition over a wide range of conditions. The properties of the standard M864 are given in Figure 1.

The flight experiments employ Doppler radar to track the trajectory; and, from these measurements and 3D modified point mass simulation, the drag and velocity of the projectile in flight are deduced. The data reduction technique and results have been reported by Lieske.[6,7] The modeling analysis developed here has been applied to some of these cases.

Figure 28 shows a comparison between the range determined by Lieske using the 3D modified point mass trajectory model where data from the Doppler radar are used to determine the drag coefficient with the gas generator operating. This figure shows shots of the standard mass projectile for three gun charges. The line, basically through the data, is the present computation. This figure shows that the computation gives the correct trend and magnitude. However, a better picture of the ability of the model can be obtained from Table 3 which also includes a fourth case of the light weight projectile launched with

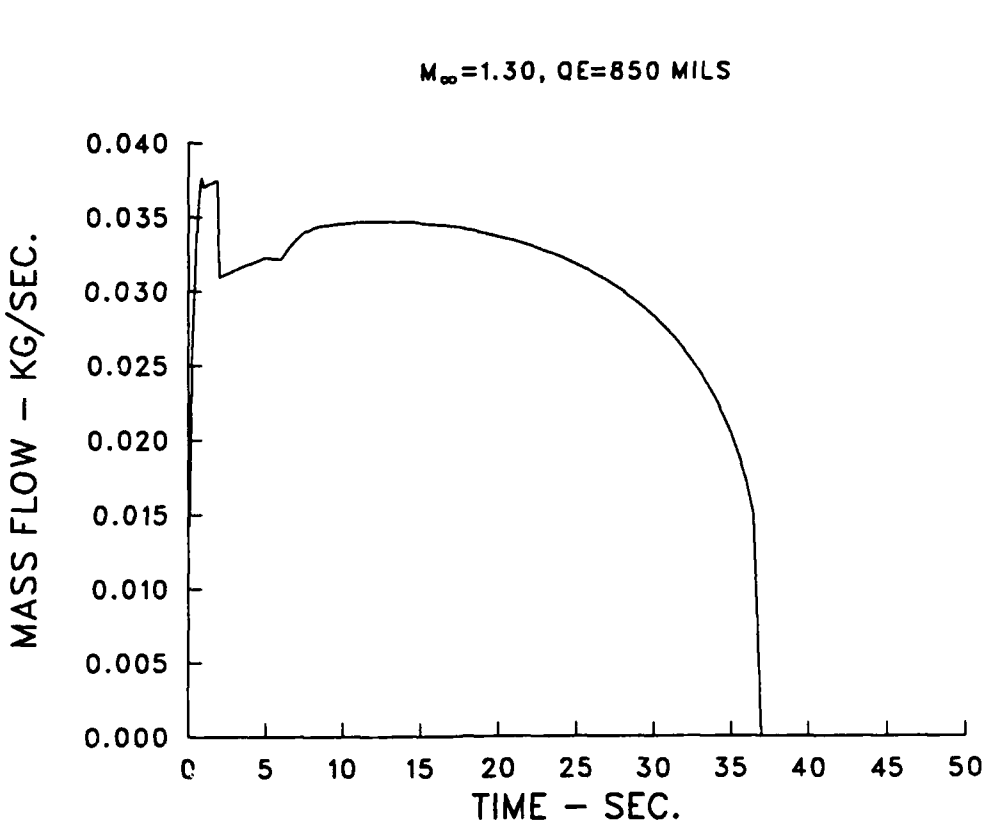

Figure 27: Mass Flow from Gas Generator for M864-L Flight

a non-standard charge. The present model agrees with that predicted by Firing Tables computation within 800 m for the four cases considered. The Firing Tables technique is an empirical fit to extensive firing data; and thus it gives ranges with an accuracy of about 0.4 per cent (100 m in 25,000 m).

TABLE 3: PREDICTED FLIGHT RANGE DATA FOR M864

QE=850. MILS				
CHARGE	M_i	RANGE COMPUTED	RANGE FIRING TABLES	DIFFERENCE
		km	km	PER CENT
6W-	1.30	12.82	12.557	+2.0
7W	1.61	17.87	17.153	+4.2
7R	1.97	22.24	21.996	+1.1
8R	2.37	27.32	28.129	-2.9

Figure 29 shows the calculated burnout time of the propellant in the M864 as a function of launch conditions. At low quadrant elevations there is relatively little variation of burnout with respect to the average time of 33 seconds. But, as the elevation increases, the projectile spends more time at high altitude and there is a significant increase in burn time and more variation with gun charge (i.e., launch Mach number). The Doppler radar measurements reported by Lieske do not show an effect of elevation or launch Mach number

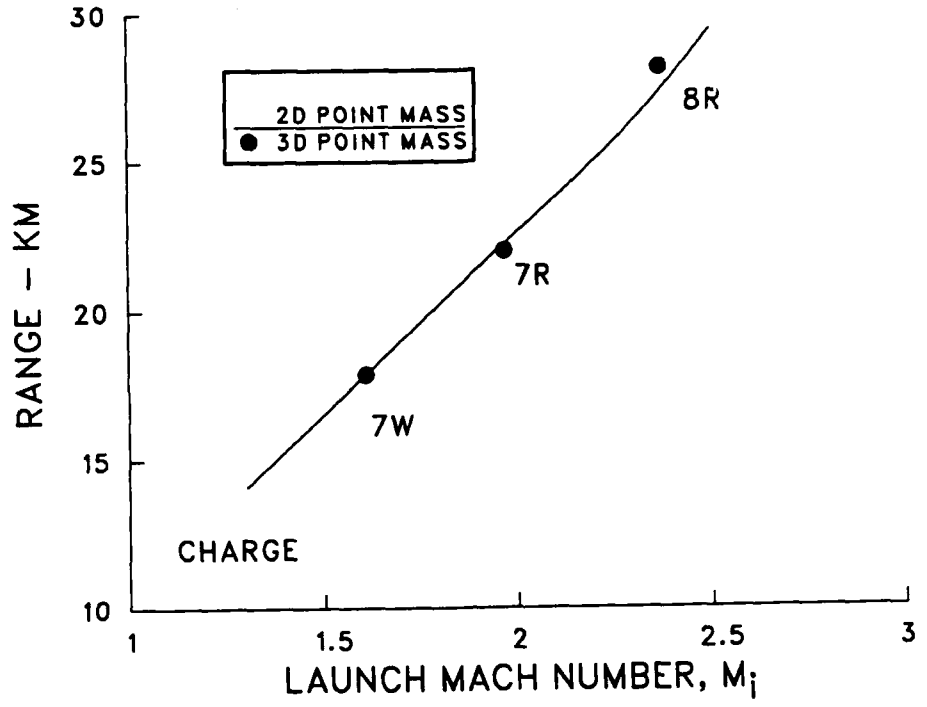

Figure 28: Computed Range Versus Launch Mach Number Compared to 3D Modified Point Mass Predictions

on the performance of the propellant. His results are best correlated using a fixed burn time of 33 seconds; however, the trajectory model deduced from the radar data indicates that the drag reduction does depend on atmospheric pressure. Computations using a lower value of n, the exponent in the effect of chamber pressure on burn rate, considerably reduces the effect of elevation on burn time. Hudgins[15] cites a value of n=0.51 as recommended by the propellant manufacturer base on tests over a limited variation in pressure.

VII. CONCLUDING SUMMARY

An engineering model for the performance of the M864 base burn projectile has been assembled and tested on a number of flight cases. The model takes into account the three main elements of the problem: gas generator mass flow prediction; the drag reduction caused by the mass injected into the wake; and a two dimensional modified point mass trajectory computation. The predictive capability is, at this point, deficient in a number of respects; but qualitative predictions are made of all the physical aspects of the system's performance. The computer model is based on laboratory experiments, analysis, and flight tests of the inert shell. No extra factors have been introduced to improve the agreement with measured data from flights of the M864 projectile.

The Navier-Stokes computations of the base flow, being carried out at the Ballistic Research Laboratory, have been a critical element in formulating a comprehensive model.

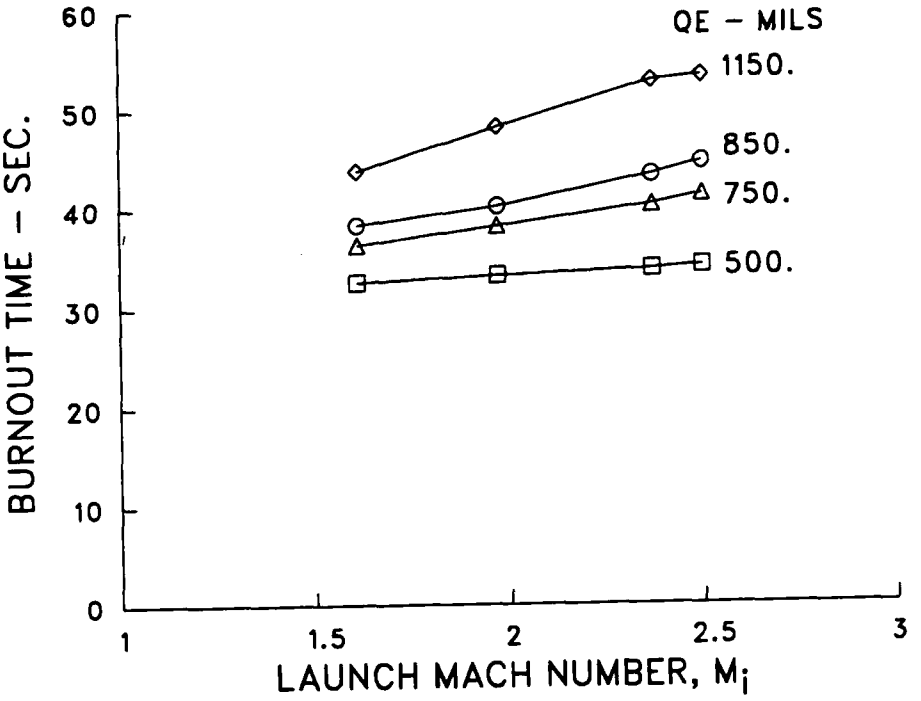

Figure 29: Computed Gas Generator Burnout Time Versus Launch Mach Number and Elevation

These computations have been used to provide a correlation of change in base pressure with mass injection, Mach number and taking into account the temperature of the gas. This later effect is of critical importance for the development of a physically realistic model of the effect of mass addition on drag reduction. Applicable data have been unavailable in previous experimental studies.

The analysis of the gas generator performance used momentum and mass conservation laws, a burning rate law developed by Miller et al, [32] and the geometry of the solid propellant grain to predict the mass flow as a function of the exit pressure of the motor. The ground based experiments with a spin fixture[5] were used to determine the effect of spin rate on the burning rates. The burning surface is divided into a cylindrical and slot surface with different burning rates on each. The cylindrical burning rate is inversely proportional to the burnout time. Thus, it increases almost linearly with spin rate according to the spin fixture tests. The slot surface burn rate is determined by the observation that, in the spin fixture tests, all chamber pressure data start at approximately the same value at the same time, independent of spin rate. A slot burn rate which almost linearly decreases with spin is necessary to satisfy that condition. The resulting chamber pressure-time histories agree reasonably well with the ground tests, especially in the early times.

The literature on the aerodynamic effect of mass addition to the near wake has been reviewed. The mass flow produced by the M864 is such that interest is focused on low values of injection rate. This suggests that the important range of the injection parameter is less than 0.005 in the supersonic flight. In that range, the linear change of base pressure with injection rate is applicable and has been determined for the existing data. When

the data are interpreted in this form, a clear Mach number correlation is observed. The Navier-Stokes computations of Nietubicz et al[40] extend the data base to include effects of elevated injected gas temperatures as well as confirming the low temperature wind tunnel data which had to be evaluated graphically. The final result of this part of the study is a correlation equation which can be used to predict the average base pressure over the range of conditions experienced by the M864. The correlation can be improved with more numerical data, particularly in the low supersonic and transonic flight regimes. The average base pressure computed from this model is used to directly determine the base drag reduction.

The ground based tests show that the gas generator performance is time, pressure and spin dependent. Thus, the computed base drag reduction depends on the projectiles trajectory. As a consequence, the analysis is completed with the incorporation of a trajectory model. A two-dimensional modified point mass method is used which employs a fourth order Runga-Kutta integration technique. The computed trajectory for the inert M864 agrees (within 60 meter in 24,000) with a full three-dimensional modified point mass method currently in use for generating firing tables.

The analytical model of the M864 has been compared with an instrumented flight test case. The measured chamber pressure and base pressure versus time are predicted by the model. The computed burnout time predicted was 36.8 seconds compared to an observed burnout of 35.3 seconds. The time of flight is also predicted within one second. One of the major problem areas is the timing of the ignition phase of the motor performance. The model was also applied to a number of flight conditions representing normal operational situations. Doppler radar data are available for these conditions and total range predictions gave correct trends and range values within 4.2 per cent of the test results.

REFERENCES

1. S.N.B. Murthy, (Ed.), Aerodynamics of Base Combustion, Progress in Astronautics and Aeronautics, Vol. 40, AIAA, New York, New York, 1976.

2. J. Bostonian, Base Bleed: "A Drag Reduction System for Cannon-Launched Projectiles," ARLCD-TR-81002, U.S. Army Armament Research and Development Command, Dover, New Jersey, August 1981 (AD B058881L).

3. J.D. Kuzan and V. Oskay, "Ignition Delay of the Solid Propellant in the M864 Base Burn Projectile," BRL-MR-3653, Ballistics Research Laboratory, Aberdeen Proving Ground, Maryland, March 1988 (AD B121544)

4. V. Oskay and J.M. Garner, "Initial Yawsonde Tests of 155 MM M864 Base-Burn Projectile," BRL-MR-3707, Ballistic Research Laboratory, Aberdeen Proving Ground, Maryland, November 1988 (AD 199984).

5. L.D. Kayser, J.D. Kuzan, and D.N. Vazquez, "Ground Testing for Base-Burn Projectile Systems," BRL-MR-3708, Ballistic Research Laboratory, Aberdeen Proving Ground, Maryland, November 1988 (AD A201107), also see Paper C-6, Proceedings of the Tenth International Symposium on Ballistics, October 1987.

6. R.F. Lieske, "Determination of Aerodynamic Drag and Exterior Ballistic Trajectory Simulation for the 155mm, DPICM, M864 Base-Burn Projectile," BRL-MR-3768, U.S. Army Ballistic Research Laboratory, Aberdeen Proving Ground, Maryland, June 1989. (AD A209510)

7. R.F. Lieske, J.A. Hurff, and J.A. Matts, "Modified Point Mass Trajectory Simulations for the 155mm, DPICM, M864 Base-Burn Projectile," to be published, U.S. Army Ballistic Research Laboratory, Aberdeen Proving Ground, Maryland.

8. J. Sahu, C.J. Nietubicz, and J.L. Steger, "Navier-Stokes Computations of Projectile Base Flow with and without Mass Injection," *AIAA Journal* Vol. 23, No. 9, September 1985, pp. 1348-1355.

9. E.F. Brown and D.B. Griggs, "Preliminary Results of Extended Range Ordnance (ERO) Risk Reduction Test," AMB-IR-4-88, Aeromechanics Branch, U.S. Army Armament Research and Development Center, Picatinny Arsenal, New Jersey, August 1988.

10. K. Andersson, N.E. Gunners, and R. Hellgren, " 'Swedish Base Bleed' -Increasing the Range of Artillery Projectiles through Base Flow," Propellants and Explosives, Vol. 1, 1976, pp. 69-73.

11. K. Lundahl and N. Bartelson, "Base Bleed - A System to Increase Range and Decrease Ballistic Disperson," 3rd International Symposium on Ballistics, Karlsruhe, 23-25 March 1977.

12. K. Andersson, N. Bartelson, and N.-E. Gunners, "Afterbody Drag of Projectiles with Base Drag Reducing Systems," 4th International Symposium on Ballistics, October 1978, pp. 17-19.

13. R.V. Hellgren, "Range Calculation for Base Bleed Projectiles," Proceedings of the 6th International Symposium on Ballistics, Amsterdam, Holland, 1984.

14. N-E Gunners, K Andersson, R. Hellgren, "Base-Bleed Systems for Gun Projectiles," Progress in Astronautics and Aeronautics, Gun Propulsion Technology, Vol. 109, Chapter 16, 1988.

15. H.E. Hudgins, "An Updated Interim Model of Base Burning Drag Reduction for the 155MM, M864 Projectile," U.S. Army Armament Research and Development Center, Picatinny Arsenal, New Jersey, 1987.

16. K.K. Kuo, J.N. Fleming, "Proceedings of First International Symposium on Special Topics in Chemical Propulsion: Base Bleed," Athens, Greece, November, 23-25, 1988.

17. P.R. Reijasse, R. Benay, J.M. Delery, and R.G. Lacau, "Missile and Projectile Base-Flow Prediction by Multi-Component Methods," AIAA Paper No. 88-4380, Atmospheric Flight Mechanics Conference, Minneapolis, MN, August 1988, pp. 438-446.

18. W. Calarese, "GAU-8 Projectile Afterbody Drag Reduction by Boattailing and Base Injection with Heat Addition," AIAA Paper No. 79-0146, Aerospace Science Meeting, January 1979.

19. H. Schilling, "Experimental Investigation on the Base-Bleed-Effect for Body-Tail-Combinations," Proceedings of the 8th International Symposium on Ballistics, Orlando, Florida, October 1985.

20. L.D. Kayser, "Effects of Base Bleed and Supersonic Nozzle Injection on Base Pressure," Memorandum Report No. 2456, USA Ballistic Research Laboratories, Aberdeen Proving Ground, Maryland, March 1975 (AD B003442L).

21. G.A. Sullins, J.D. Anderson, and J.P. Drummond, "Numerical Investigation of Supersonic Base Flow with Parallel Injection," AIAA Paper No. 82-1001, June 1982.

22. R.J. Cavalleri, "Base Drag Reduction Using Angled Injection," ATA-87-001, Applied Technology Associates, Orlando, Florida, June 1987.

23. J.A. Schetz, F.S. Billig, and S. Favin, "Simplified Analysis of Supersonic Base Flows including Injection and Combustion," AIAA Journal, Vol. 14, No. 1, January 1976, pp 7-8.

24. J.A. Schetz, S. Favin, and F.S. Billig, "Analytical Comparison of the Performance of Different Base-Burning Modes," AIAA Journal, Vol. 14, No. 9, September 1976, pp 1337-1338.

25. J.A. Schetz, F.S. Billig, and S. Favin, "Approximate Analysis of Base Burning in Supersonic Flow," Progress in Astronautics and Aeronautics, Vol. 40, 1976, p. 385.

26. J.E. Hubbartt, W.C. Strahle, and D.H. Neale, "Mach 3 Hydrogen External/Base Burning," AIAA Journal, Vol. 19, June 1981, pp. 745-749.

27. W.C. Strahle, J.E. Hubbartt, and R. Walterick, "Base Burning Performance at Mach 3," AIAA Journal, Vol. 20, No. 7, July 1982, pp 986-991.

28. W.C. Strahle, and J.E. Hubbartt, "Base and External Burning for Propulsion," AGARD 58th Symposium on Ramjets and Ramrockets for Military applications, October 1981.

29. D.H. Neale, J.E. Hubbartt, W.C. Strahle, and W.W. Wilson, "Experiments and Analysis Related to External Burning for Propulsion," Air Force Office of Scientific Research, Washington, D.C., AFOSR-TR-0602, March 1977.

30. K.C. Schadow and D.J. Chieze, "Simulation of External Burning in a Two-Dimensional, Planar Wind Tunnel," 14th JANNAF Combustion Conference, Colorado Springs, Colorado, August 15-19, 1977.

31. K.C. Schadow and D.J. Chieze, "Experimental Investigation of Combined Base Injection and External Burning," AIAA Journal, Vol. 16, No. 10, October 1978, pp. 1084-1089.

32. M.S. Miller and H.E. Holmes, "An Experimental Determination of Subatmospheric Burning Rates and Critical Diameters for AP/HTPB Propellant," Proceedings of the 1987 JANNAF Combustion Meeting, Monterrey, California, October 1987.

33. M.J. Zucrow and J.D. Hoffman, Gas Dynamics, Vol 1, John Wiley and Sons, Inc. New York, 1976, p. 197.

34. A.H. Shapiro, The Dynamics and Thermodynamics of Compressible Flow, Vol. 1, Ronald Press, New York, 1953, p. 100.

35. D.J. Collins, L. Lees, and A. Roshko, "Near Wake of a Hypersonic Blunt Body with Mass Addition," AIAA Journal, Vol. 8, No. 5, May 1970, pp. 833-842.

36. J.E. Bowman and W.A. Clayden, "Cylinderical Afterbodies in Supersonic Flow with Gas Ejection," AIAA Journal, Vol. 5, No. 8, August 1967, pp 1524-1525.

37. W.A. Clayden and J.E. Bowman, "Cylindrical Afterbodies at M_∞=2 with Hot Gas Ejection," AIAA Journal, Vol. 6, No. 12, December 1968, pp 2429-2431.

38. J. Reid and R. Hastings, "The Effect of a Central Jet on the Base Pressure of a Cylindrical Afterbody in Supersonic Stream," Royal Aircraft Establishment, Farnborough, England, Report AERO 2621, December 1959.

39. D.M. Sykes, "Cylindrical and Boattailed Afterbodies in Transonic Flow with Gas Ejection," AIAA Journal, Vol. 8, No. 3, March 1970, pp. 588-589.

40. C.J. Nietubicz, and J. Sahu, "Navier-Stokes Computations of Base Bleed Projectiles," Paper No. II-2, First International Symposium on Special Topics in Chemical Propulsion: Base Bleed, Athens, Greece, November, 23-25, 1988.

41. J. Sahu, "Supersonic Flow over Cylindrical Afterbodies with Base Bleed," BRL-TR-2740, US Army Ballistic Research Laboratory, Aberdeen Proving Ground, Maryland, June 1986 (AD 171461).

42. Z. Ding, Y. Liu and S. Chen, "A Study of Drag Reduction by Base Bleed at Subsonic Speeds," First International Symposium on Special Topics in Chemical Propulsion: Base Bleed, Athens, Greece, November, 23-25, 1988.

43. L.H. Townend and J. Reid, "Some Effects of Stable Combustion in Wakes Formed in a Supersonic Stream" in Supersonic Flow, Chemical Processes and Radiative Transfer, Ed. D.B. Olfe and V. Zakkay, Pergamon Press, 1964, p. 137.

44. V. Oskay and J. Kuzan, "Results from The Transonic Range Firing Program for The 155MM M864 Base-Burn Projectile," to be published, U.S. Army Ballistic Research Laboratory, Aberdeen Proving Ground, Maryland, 1989.

45. R. Sahu, Unpublished M864 computations, 1988.

46. R.F. Lieske, and M.L. Reiter, "Equations of Motion for a Modified Point Mass Trajectory," BRL Report No. 1314, U.S. Army Ballistic Research Laboratory, Aberdeen Proving Ground, Maryland, March 1966 (AD 485869).

47. NATO STANAG 4355 (Draft Edition 1), The Modified Point Mass Trajectory Model, February 1988.

48. L.D. Kayser, J.D. Kuzan, and D.N. Vazquez, "Flight Testing for 155MM Base Burn Projectile," BRL-MR-3708, U.S. Army Ballistic Research Laboratory, Aberdeen Proving Ground, Maryland, November 1988. (AD A201107) Also see Conference Proceedings 89-2208, AIAA 7th Applied Aerodynamics Conference, Seattle, WA., July 31-Aug 2 1989, pp408-416.

LIST OF SYMBOLS

a	Grain surface area
A	Area
A_b	Base area
A_e	Exit area
A_{ref}	Reference area (projectile maximum cross section)
C_D	Drag coefficient
C_{D_b}	Base drag coefficient
C_{D_o}	Zero yaw total drag coefficient
$C_{D_{pv}}$	Forebody pressure and friction drag coefficient
$C_{D_{\alpha^2}}$	Yaw squared drag coefficient
C_{l_p}	Spin damping coefficient
C_{M_α}	Slope of the pitching moment curve
$C_{Y_{p\alpha}}$	Magnus force coefficient
C_v	Discharge coefficient
D	Diameter
f_o	Strand burning rate correction factor at zero spin
f_c	Cylindrical surface burning rate correction factor to account for the effect of spin
f_s	Slot surface burning rate correction factor to account for effect of spin
f_{dr}	Drag reduction factor
g	Acceleration of gravity
I	Non-dimensional injection rate
I_x	Axial Moment of inertia
K	Constant
k	Constant in burning rate versus pressure formula
l	Length of the propellant grain
M_∞	Free-stream Mach number
m	Mass
$\dot{m}$	Mass flow
n	Exponent in burning rate versus pressure formula
P	Pressure
P_c	Combustion chamber pressure
p	Spin rate
R_{earth}	Radius of the earth
r	Radius of the propellant grain
r_{mx}	Maximum radius of the propellant grain
r_s	End corner radius of the propellant grain
$\dot{r}$	Burning rate
$\dot{r}_o$	Burning rate observed in strand burning tests
T	Temperature
T_c	Combustion chamber temperature
t	Time
u	Velocity component in the x direction
u_e	Exit velocity of combustion products
V	Magnitude of the projectile velocity

$\vec{V}$	Vector velocity
v	Velocity component in y direction
w	Slot width
x	Distance down range
x_	Down range distance at previous time step
y	Height (altitude)

Greek Symbols

α_e	Yaw of repose
β	Nonlinear parameter in base pressure versus I
γ_g	Ratio of specific heats of combustion products
θ	Parameter in propellant grain surface area computation
Δx	Range change computed from ecceleration
ρ	Density
σ	Slope $\frac{d(P_b/P_\infty)}{dI}$

Subscripts

b	Base
c	Cylinder
e	Exit
i	Initial
j	Injected gas
ref	Reference
sl	Sea level
s	Slot
1	End of ingnition transient
∞	Free-stream

No of Copies	Organization
1	Office of the Secretary of Defense OUSD(A) Director, Live Fire Testing ATTN: James F. O'Bryon Washington, DC 20301-3110
(Unclass., unlimited) 12 (Unclass., limited) 2 (Classified) 2	Administrator Defense Technical Info Center ATTN: DTIC-DDA Cameron Station Alexandria, VA 22304-6145
1	HQDA (SARD-TR) WASH DC 20310-0001
1	Commander US Army Materiel Command ATTN: AMCDRA-ST 5001 Eisenhower Avenue Alexandria, VA 22333-0001
1	Commander US Army Laboratory Command ATTN: AMSLC-DL Adelphi, MD 20783-1145
2	Commander Armament RD&E Center US Army AMCCOM ATTN: SMCAR-MSI Picatinny Arsenal, NJ 07806-5000
2	Commander Armament RD&E Center US Army AMCCOM ATTN: SMCAR-TDC Picatinny Arsenal, NJ 07806-5000
1	Director Benet Weapons Laboratory Armament RD&E Center US Army AMCCOM ATTN: SMCAR-CCB-TL Watervliet, NY 12189-4050
1	Commander US Army Armament, Munitions and Chemical Command ATTN: SMCAR-ESP-L Rock Island, IL 61299-5000
1	Commander US Army Aviation Systems Command ATTN: AMSAV-DACL 4300 Goodfellow Blvd. St. Louis, MO 63120-1798

No of Copies	Organization
1	Director US Army Aviation Research and Technology Activity Ames Research Center Moffett Field, CA 94035-1099
1	Commander US Army Missile Command ATTN: AMSMI-RD-CS-R (DOC) Redstone Arsenal, AL 35898-5010
1	Commander US Army Tank-Automotive Command ATTN: AMSTA-TSL (Technical Library) Warren, MI 48397-5000
1	Director US Army TRADOC Analysis Command ATTN: ATAA-SL White Sands Missile Range, NM 88002-5502
(Class. only) 1	Commandant US Army Infantry School ATTN: ATSH-CD (Security Mgr.) Fort Benning, GA 31905-5660
(Unclass. only) 1	Commandant US Army Infantry School ATTN: ATSH-CD-CSO-OR Fort Benning, GA 31905-5660
1	Air Force Armament Laboratory ATTN: AFATL/DLODL Eglin AFB, FL 32542-5000
	Aberdeen Proving Ground
2	Dir, USAMSAA ATTN: AMXSY-D AMXSY-MP, H. Cohen
1	Cdr, USATECOM ATTN: AMSTE-TD
3	Cdr, CRDEC, AMCCOM ATTN: SMCCR-RSP-A SMCCR-MU SMCCR-MSI
1	Dir, VLAMO ATTN: AMSLC-VL-D

No. of Copies	Organization
3	Commander Naval Surface Warfare Center ATTN: Code R44, Dr. F. Priolo Code R44, Dr. A. Wardlaw K24, B402-12, Dr. W. Yanta White Oak Laboratory Silver Spring, MD 20903-5000
1	United States Military Academy Department of Mechanics ATTN: LTC Andrew L. Dull West Point, NY 10996
1	US Naval Weapons Center Aerothermochemistry Division ATTN: Dr. K. C. Schadow China Lake, CA 93555
10	Commander Armament RD&E Center US Army AMCCOM ATTN: SMCAR-TSS SMCAR-FSA-F, R. DeKleine R. Kline F. Brody R. Botticelli P. DeMasi H. Hudgins J. Grau S. Kahn Dr. J. Rubin Picatinny Arsenal, NJ 07806-5000
1	Commander US Naval Surface Warfare Center ATTN: Dr. F. Moore Dahlgren, VA 22448
1	Air Force Armament Laboratory ATTN: AFATL/FXA, Stephen C. Korn Eglin AFB, FL 32542-5434
2	USAF Wright Aeronautical Laboratories ATTN: AFWAL/FIMG, Mr. Norman E. Scaggs Dr. J. Shang Wright Patterson AFB, OH 45433-6553

No. of Copies	Organization
1	Commander US Army Armament, Munitions and Chemical Command ATTN: AMSMC-PDC, L. Randol Rock Island, IL 61299-5000
4	Director National Aeronautics and Space Administration Langley Research Center ATTN: Technical Library Mr. D. M. Bushnell Dr. M. J. Hemsch Dr. I. E. Beckwith Langley Station Hampton, VA 23665
5	Director National Aeronautics and Space Administration Ames Research Center ATTN: MS-227-8, L. Schiff MS-258-1, T. Holst MS-258-1, D. Chaussee MS-258-1, M. Rai MS-229-1, M. Rubesin Moffett Field, CA 94035
2	David Taylor Research Center ATTN: Dr. P. S. Granville Dr. de los Santos Bethesda, MD 20084
2	Director Sandia National Laboratories ATTN: Dr. W. L. Oberkampf Dr. F. Blottner Division 1556 P. O. Box 5800 Albuquerque, NM 87185
2	Morton Thiokol, Inc. Elkton Division ATTN: Mr. James W. Powers Mr. Bruce Brooks P. O. Box 241 Elkton, MD 21921-0241
2	Honeywell, Inc. ATTN: Wilford E. Martwick Ken Sundeen 600 Second Street, North East Hopkins, MN 55343
2	Ford Aerospace and Communications Corporation Aeronautics Division ATTN: Charles White Bud Blair Ford Road Newpoint Beach, CA 92658

No. of Copies	Organization
2	Scientific Research Associates ATTN: Dr. Howard Gibeling Dr. Richard Buggeln 50 Nye Road, P. O. Box 1058 Glastonbury, CT 06033
1	Applied Technology Associates ATTN: Mr. R. J. Cavalleri P. O. Box 19434 Orlando, FL 32814
1	AEDC Calspan Field Service ATTN: MS 600, Dr. John Benek AAFS, TN 37389
1	Massachusetts Institute of Technology ATTN: Technical Library 77 Massachusetts Avenue Cambridge, MA 02139
1	Virginia Polytechnic Institute and State University ATTN: Dr. Clark H. Lewis Department of Aerospace and Ocean Engineering Blacksburg, VA 24061
2	University of California, Davis Department of Mechanical Engineering ATTN: Prof. H. A. Dwyer Prof. J. Steger Davis, CA 95616
1	Pennsylvania State University Department of Aerospace Engineering ATTN: Dr. G. S. Dulikravich University Park, PA 16802
1	University of Illinois at Urbana Champaign Department of Mechanical and Industrial Engineering Urbana, IL 61801
1	University of Maryland Department of Aerospace Engineering ATTN: Dr. J. D. Anderson, Jr. College Park, MD 20742
1	University of Notre Dame Department of Aeronautical and Mechanical Engineering ATTN: Prof. T. J. Mueller Notre Dame, IN 46556

No. of Copies	Organization
1	University of Texas Department of Aerospace Engineering and Engineering Mechanics ATTN: Dr. D. S. Dolling Austin, Texas 78712-1055
2	University of Delaware Department of Mechanical Engineering ATTN: Dr. John Meakin, Chairman Dr. Barry Sidel Newark, DE 19716
1	The University of Arizona Aerospace Engineering Department ATTN: Prof. I. Wygnanski Tucson, AZ 85721
1	University of Cincinnati Department of Aerospace Engineering ATTN: Prof. Stanley Rubin Mail Location 70 Cincinnati, OH 45221
1	Illinois Institute of Technology College of Engineering Fluid Dynamics Research Center ATTN: Dr. Mukund Acharya IIT Center Chicago, Il 60616
1	University of New Mexico Department of Mechanical Engineering ATTN: Dr. C. Randall Truman Albuquerque, New Mexico 87131
1	Pennsylvania State University Department of Mechanical Engineering ATTN: Dr. Kenneth Kuo University Park, PA 16802
1	Florida Atlantic University Department of Mechanical Engineering ATTN: Dr. W. L. Chow Boca Raton, FL 33431
1	Georgia Institute of Technology School of Aerospace Engineering ATTN: Dr. Warren C. Strahle Atlanta, GA 30332

No. of Copies	Organization
1	TECHNION Aeronautical Engineering Department ATTN: Dr. A. Sigal Haifa 32 000 ISRAEL
2	National Defence Research Institue Department 2 (FOA 022) ATTN: Dr. R. Hellgren Dr. N-E. Gunners Fack, 104 50 Stockholm SWEDEN
2	Rheinmetall GmbH ATTN: Dr. Schilling Dr. L. Borngen Ulmen Strasse 125, D-4000 Dusseldorf 30, WEST GERMANY
2	Royal Armament Research and Development Establishment ATTN: Dr. C. N. Bowden Dr. G. I. Lindsley, GS2 Div. Fort Halstead, Sevenoaks, Kent, TN14 7BP UNITED KINGDOM
1	Ecole Royale Militaire ATTN: Prof. E. Celens Avenue de La Renaissance 30, 1040 Bruxelles, BELGIUM
1	Proof and Experimental Test Establissment ATTN: Mr. L. W. Desfosses P. O. Box 2220 Nicolet, Quebec CANADA
1	Establissment Techn. Bourges ATTN: Mr. D. Chargelegue BP 712 18015 Bourges Cedex FRANCE
1	Haerens Artilleriskole ATTN: Mr. F. H. Valeur Postboks 182 DK-6800 Varde DENMARK
1	BWB-WM II 6 ATTN: Mr. V. Buhner Konrad Adenauer Ufer 2-6 54 Koblenz GERMANY

No. of Copies	Organization
1	DMKL/MBA-1 ATTN: MAJ P.L.M. Snel P. O. Box 90701 2509 LS The Hague NETHERLANDS
1	FFI ATTN: COL D. Cappelen P. O. Boks 25 N-2007 Kjeller NORWAY

USER EVALUATION SHEET/CHANGE OF ADDRESS

This Laboratory undertakes a continuing effort to improve the quality of the reports it publishes. Your comments/answers to the items/questions below will aid us in our efforts.

1. BRL Report Number BRL-TR-3096 Date of Report APRIL 1990

2. Date Report Received _____

3. Does this report satisfy a need? (Comment on purpose, related project, or other area of interest for which the report will be used.) _____

4. Specifically, how is the report being used? (Information source, design data, procedure, source of ideas, etc.) _____

5. Has the information in this report led to any quantitative savings as far as man-hours or dollars saved, operating costs avoided, or efficiencies achieved, etc? If so, please elaborate. _____

6. General Comments. What do you think should be changed to improve future reports? (Indicate changes to organization, technical content, format, etc.) _____

CURRENT ADDRESS

Name

Organization

Address

City, State, Zip Code

7. If indicating a Change of Address or Address Correction, please provide the New or Correct Address in Block 6 above and the Old or Incorrect address below.

OLD ADDRESS

Name

Organization

Address

City, State, Zip Code

(Remove this sheet, fold as indicated, staple or tape closed, and mail.)

---FOLD HERE---

DEPARTMENT OF THE ARMY
Director
U.S. Army Ballistic Research Laboratory
ATTN: SLCBR-DD-T
Aberdeen Proving Ground, MD 21005-5066
OFFICIAL BUSINESS

NO POSTAGE
NECESSARY
IF MAILED
IN THE
UNITED STATES

BUSINESS REPLY MAIL
FIRST CLASS PERMIT No 0001, APG, MD

POSTAGE WILL BE PAID BY ADDRESSEE

Director
U.S. Army Ballistic Research Laboratory
ATTN: SLCBR-DD-T
Aberdeen Proving Ground, MD 21005-9989

---FOLD HERE---